Study of the COMPASS spectrometer performance using K_S^0 events

Karin Schoenning

CERN, Geneva 2003

Master of Science Thesis

Uppsala University, Sweden

Department of Radiation Science

Abstract

In this diploma thesis, the performance of the COMPASS spectrometer was investigated, by studying muon-nucleon scattering events where K_S^0 mesons were produced. The K_S^0 yield per event is around 0.46 % depending on the run number. Most of the results are obtained from DST4 data from the run period P2D in year 2002. The distributions of primary and secondary vertices were studied and an unsatisfactory feature of the vertex reconstruction was discovered. The sample of K_S^0 meson candidates was subdivided into classes depending on the location of the decay vertex. The reconstructed mass distribution of the K_S^0 meson was analysed and it was found that the reconstructed mass is shifted with respect to the PDG value. The magnitude and the sign of the shift depend on where the K_S^0 meson decays, where in the spectrometer the decay product tracks end and from which run the data come. The measured K_S^0 mass resolution is larger than the K_S^0 mass errors calculated from the decay pion track parameters. The measured mass resolution depends on the location of decay vertex, on the position of the decay track endpoints and on the run from which the data come.

Contents

1 INTRODUCTION

One of the presently most challenging problems of particle physics is to understand the spin structure of the nucleon. An important tool for this is the polarised deep inelastic lepton-nucleon scattering. The first experiment with a high energy polarised electron beam was initiated by V.W Hughes and performed at SLAC in the mid-seventies. This gave results in agreement with the Quark Parton Model and confirmed the Bjorken sum rule and the Ellis-Jaffe sum rule for the proton [1]. The EMC experiment at CERN in the in the mid-eighties made use of a tenfold higher beam energy. That allowed for measurements at much lower values of the Bjorken scaling variable x. They showed a violation of the Ellis-Jaffe sum rule for the proton in the extended kinematic region [2]. This was a hint that the naive Quark Parton Model, where the nucleon is built up by its three valence quarks carrying all its momentum and spin, was not entirely true. New experiments using polarised deep inelastic scattering were performed to investigate this further, among others the SMC at CERN that gave results in agreement with the EMC. Similar results were also found for the neutron [3]. The spin dependent structure functions have been studied which has resulted in suggestions that it is only at the naive parton level that the total spin of the nucleon is carried by quarks. The gluons inside the nucleon might also be polarised. They would thereby contribute to the total nucleon spin, together with the angular momentum of the quarks and the gluons inside the nucleon. How to measure the latter is not yet known, but one of the main tasks for the COMPASS experiment is to measure the polarisation of the gluon for the proton and the neutron [4]. The NA58 COMPASS (COmmon Muon and Proton Apparatus for Structure and Spectroscopy) experiment is performed at CERN. The photon-gluon fusion process (PGF) leading to open charm production will be investigated. A polarised muon beam and a polarised nucleon target is being used for this purpose, as well as a two-staged spectrometer. So far, data taking has been going on during 2001 and 2002, whereof the main purpose of the 2001 data taking was to examine the general performance of the experiment. The 2002 data are to be used for the physics programmes; one of them is the measurement of the gluon polarisation. However, there are still features of the spectrometer performance and the data reconstruction that need to be understood. To achieve this, the production of K^0_S mesons in the μN interactions is studied. The properties of the K^0_S meson are well known, which makes it a suitable tool for this purpose.

This paper is organised as follows: In section 2, a brief description of the method used by COMPASS to measure the gluon polarisation is given. This is followed by a presentation of the COMPASS experimental setup in section 3. Then, in section 4, the methods used for studying the spectrometer performance are described. In section 5 the data sample is presented. The results are given in section 6 and finally the conclusions in section 7.

2 POLARISATION OF THE GLUON

The gluon polarisation is defined as $\Delta G/G$ where $\Delta G = \int_0^1 \Delta g(x,Q^2)dx$, $G = \int_0^1 g(x,Q^2)dx$ and $\Delta g(x,Q^2)$ and $g(x,Q^2)$ are the polarised and unpolarised gluon distributions in the nucleon, respectively. The gluon polarisation can be measured in different ways: by QCD evolution of the spin dependent structure function $g_1(x,Q^2)$, by selecting events with correlated hadron pairs of high transverse momenta and by measuring the longitudinal spin asymmetry of open charm leptoproduction. The first way is difficult because the spin dependent structure functions are poorly known in the low x region. The second way will be used in the spin experiments at the Relativistic Heavy Ion Collider (RHIC) at the Brookhaven National Laboratory and the last way in COMPASS.

Polarised deep inelastic scattering experiments such as COMPASS measure spin assymmetries

$$A(x,Q^2) = \frac{\Delta\sigma(x,Q^2)}{2\sigma(x,Q^2)} \tag{1}$$

where $\Delta\sigma$ (σ) is the spin dependent (spin average) cross section for lepton-nucleon scattering. They are given by

$$\Delta\sigma(x,Q^2) = \sigma^{\leftarrow\rightarrow}(x,Q^2) - \sigma^{\leftarrow\leftarrow}(x,Q^2) \tag{2}$$

$$\sigma(x,Q^2) = \frac{1}{2}(\sigma^{\leftarrow\rightarrow}(x,Q^2) + \sigma^{\leftarrow\leftarrow}(x,Q^2)) \tag{3}$$

where the arrows correspond to respective orientations of the beam and target particle spins [5]. The spin dependent cross sections depend on polarised gluon distributions $\Delta g(x,Q^2)$ in the leading order [4] and can, in the case of PGF, be measured by tagging open charm events. PGF dominates the production of open charm, since the relatively large mass of the charm quark makes it unlikely as a sea quark. The PGF process is shown in Figure 1.

In the COMPASS experiment, muons of energy 160 GeV are scattered off a polarised proton or deuteron target. The detection of open charm hadrons in the final state will mainly be done by identifying D^0 and $\overline{D}^0$ through their decay channels $D^0 \to K^-\pi^+$ and $\overline{D}^0 \to K^+\pi^-$ [4]. To improve statistics, other open charm channels can be included, like $D^+ \to K^+\pi^+\pi^-$ and in particular $D^{*+} \to D^0\pi^+$.

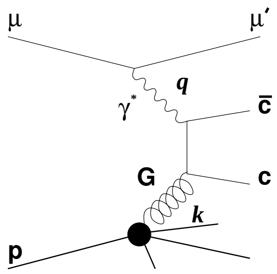

Figure 1: The photon gluon fusion diagram [4]

The measured spin asymmetry is

$$A^{meas} = \frac{N_{c\bar{c}}^{\leftarrow\rightarrow} - N_{c\bar{c}}^{\leftarrow\leftarrow}}{N_{c\bar{c}}^{\leftarrow\rightarrow} + N_{c\bar{c}}^{\leftarrow\leftarrow}} = p_B p_T f D A_{c\bar{c}}^{\gamma^* N} \tag{4}$$

where $N_{c\bar{c}}^{\leftarrow\leftarrow}$ ($N_{c\bar{c}}^{\leftarrow\rightarrow}$) is the number of events with target spin parallel (antiparallel) to the muon helicity, D is the depolarisation factor of the virtual photon, p_T and p_B are the polarisations of the target and the beam, respectively, and f is the fraction of polarisable material in the target. $A_{c\bar{c}}^{\gamma^* N}$ relates the spin dependent and the spin independent γ^*-nucleon cross sections according to

$$A_{c\bar{c}}^{\gamma^* N} = \frac{\Delta\sigma_{c\bar{c}}^{\gamma^* N}}{\sigma_{c\bar{c}}^{\gamma^* N}} \tag{5}$$

where the cross sections $\Delta\sigma_{c\bar{c}}^{\gamma^* N}$ ($\sigma_{c\bar{c}}^{\gamma^* N}$) can be expressed through the convolution of photon-gluon cross sections $\Delta\sigma(s)^{\gamma^* g \rightarrow c\bar{c}}$ ($\sigma(s)^{\gamma^* g \rightarrow c\bar{c}}$) and the gluon distribution $\Delta G(x, s)$ ($G(x, s)$) in the nucleon. Assuming that all the spin independent nucleon properties are known, the gluon polarisation can then be extracted using

$$\int_{4m_c^2}^{2M\nu} \Delta\sigma(s)^{\gamma^* g \rightarrow c\bar{c}} \Delta G(x, s) ds = A_{c\bar{c}}^{\gamma^* N} \int_{4m_c^2}^{2M\nu} \sigma(s)^{\gamma^* g \rightarrow c\bar{c}} G(x, s) ds \tag{6}$$

Here, $\sigma(s)^{\gamma^* g \rightarrow c\bar{c}}$ and $\Delta\sigma(s)^{\gamma^* g \rightarrow c\bar{c}}$ are known from QCD calculations in next to leading order and in leading order, respectively [4], ν is the energy difference between the incoming and the scattered muon, s the invariant mass squared of the photon-gluon system, m_c the mass of the charm quark and

M the nucleon mass. The statistical accuracy of the measurement of $A_{c\bar{c}}^{\gamma^* N}$ is given by

$$\delta A_{c\bar{c}}^{\gamma^* N} = \frac{1}{p_T p_B f D} \frac{1}{\sqrt{N^S}} \sqrt{1 + \frac{N^B}{N^S}} \tag{7}$$

where N^S is the number of events in the signal and N^B in the background [4].

3 THE COMPASS EXPERIMENT

3.1 The beam

A search for the gluon polarisation by photon-gluon fusion demands a polarised high energy muon beam and a polarised target. The muon beam is produced by letting high energy protons from the SPS accellerator hit a beryllium target so that charged pions and kaons, among other particles, are produced. A bending magnet selects pions and kaons with certain momenta, which later decay into muons. Due to the parity violating nature of the pion and kaon decay, the decay muon is naturally longitudinally polarised. In that way, a muon beam with intensity $2.8 \cdot 10^8 \mu^+$/spill and a momentum of around 160 GeV/c can be produced with a negative polarisation of about 80% [4].

3.2 The polarised target

The target is polarised through the Dynamic Nuclear Polarisation [6], for which low temperatures and strong magnetic fields are required. To obtain and conserve high polarisation, temperatures of the order 30 to 50 mK are needed and they are achieved using a ^3He - ^4He dilution refrigerator. The target material, ammonia NH_3 for the case of polarised protons and lithium deuteride ^6LiD for the case of polarised deuterons, is contained in two cylindrical target cells, each 60 cm long and 3 cm in diameter. The target cells are oppositely polarised and separated by a 10 cm gap. Since the target cells are situated one after the other, they are both, at the same time, exposed to the same muon beam, which makes the cross section asymmetries independent of the muon flux. A solenoid magnet supplies a magnetic field of 2.5 T, necessary for the polarisation. The field can be rotated in order to change the target polarisations, which is done 2-3 times per day, to even out false asymmetries in the open charm production. There is only a fraction of all the material in the target that is polarisable. For NH_3 this fraction, called

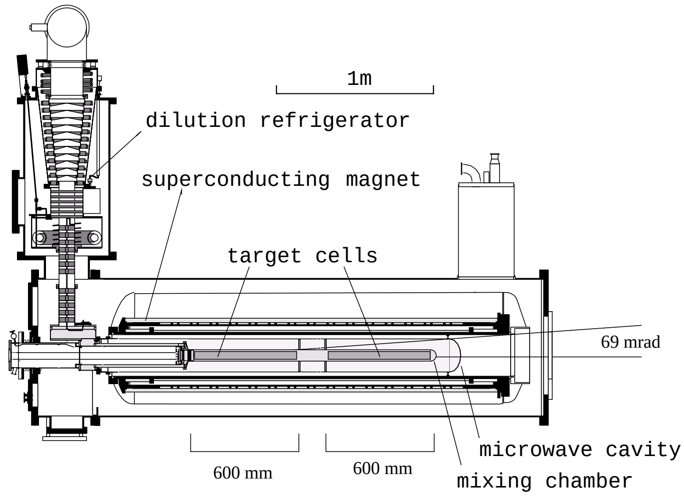

Figure 2: The COMPASS polarised target [4]

the dilution factor f (see section 2), is around 0.17 and for ^6LiD it is around 0.5 (see [5] for more details). In NH_3, the protons can be polarised up to 98%, while for ^6LiD a deuteron polarisation of around 50% [6] is achieved. The target is shown in Figure 2.

3.3 The spectrometer

The COMPASS spectrometer is a two-stage forward magnetic spectrometer. During the 2002 data taking the second RICH detector, the EM calorimetry and the large area tracking were still missing. The spectrometer is optimised for high rates and large angular acceptances required for the physics programmes. The first spectrometer stage is the large angle spectrometer (LAS) for detection of tracks with low momenta and with angles larger than 30 mrad with respect to the beam. The second stage is a small angle spectrometer (SAS), that detects tracks with angles smaller than 30 mrad and larger momenta. The spectrometer has to be two-staged in order to measure produced hadrons and scattered muons in an efficient way. The now completed SMC experiment made use of a one-stage spectrometer, which is found to be insufficient for the purposes of the COMPASS. The detection principles for the two spectrometers are essentially the same: a particle's momentum

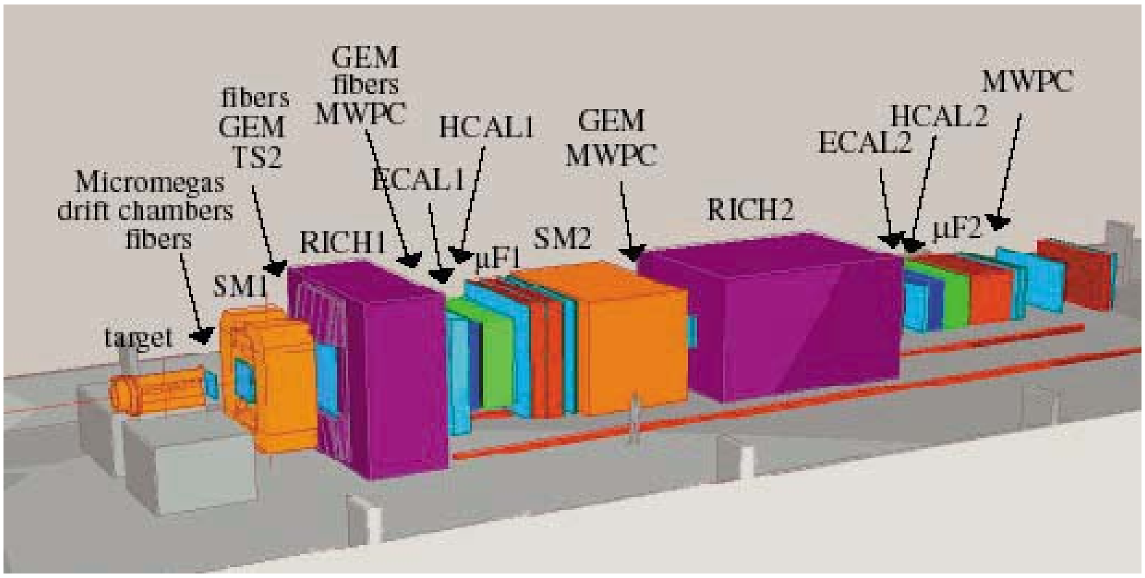

Figure 3: The proposal setup of the COMPASS spectrometer. Some parts did not operate during the 2002 data taking, as mentioned in the text.

is obtained by measuring its deflection in a magnetic field. The deflection is measured with tracking stations installed upstream and downstream of the bending magnets [7]. There are many different types of tracking detectors to optimise the efficiency for different angular ranges. For small angles, a track will be close to the beam and a detector registering it must thus be designed for the high intensity of the beam and the high tracking rate. For larger angles this is not required and another, more efficient type of tracker can be chosen. Very small angle tracking is performed by Scintillation Fibres (SciFi or FI) and Silicon Microstrips (SI), while Gas Electron Multipliers (GEM or GM) perform the small angle tracking and Drift Chambers (DC), Straw Tubes (ST) and Micro Mesh gas detectors (Micromegas or MM) the large angle tracking. The Multi Wire Proportional Chambers (MWPC) perform tracking in the whole spectrometer. To distinguish muons from other particles, two muon filters (μF1 and μF2) are applied. The principle of both of them is to absorb hadrons and register the particles that pass through the filter. The purpose of the Ring Imaging Cherenkov counter (RICH) is to identify the charged particles whose momenta are known. The RICH1 in COMPASS can separate pions, kaons and protons in the momentum range from 3 to 60 GeV/c. During the data taking of 2002, only the two hadronic calorimeters HCAL1 and HCAL2 were operating. In Figure 3 the proposal setup of the spectrometer is shown. For a detailed decription of the apparatus, see [7].

4 TOOLS FOR STUDYING THE SPECTROMETER PERFORMANCE

4.1 Motivation

To gain a deeper understanding of the properties of the spectrometer performance and of the data reconstruction, an analysis of the neutral kaon production and properties is performed. The K^0 and $\overline{K^0}$ doublet is an eigenstate of the strong and the electromagnetic interactions, but not of the weak interaction. In the weak interaction, strangeness is not conserved and there is no way of distinguishing K^0 from $\overline{K^0}$ [8]. Therefore, the experimentally observed states are linear combinations of K^0 and $\overline{K^0}$ that are CP eigenstates with $CP = 1$ and $CP = -1$. They are called K_S^0 (K_{short}) and K_L^0 (K_{long}) respectively, due to their different lifetimes. Since the lifetime of the K_L^0 is too long ($\tau = (5.17 \pm 0.04) \cdot 10^{-8}$ s) for it to decay within the COMPASS spectrometer, it is not a suitable particle for this study. The K_S^0 meson decays into states with $CP = 1$, whereof the most important decay modes are $K_S^0 \rightarrow \pi^+\pi^-$ with a fraction of 68.61% and $K_S^0 \rightarrow \pi^0\pi^0$ with a fraction of 31.39% [9]. The former is the one of interest here since the fact that the decay products are charged makes it easier to detect. The lifetime is $\tau = (0.8926 \pm 0.0012) \cdot 10^{-10}$ s, which makes the mass uncertainty, i.e. the width of the mass peak of the order of 10^{-6} eV. Compared to experimental errors, this is neglibly small. Thus the width of the peak in the mass distribution of the K_S^0 obtained in the experiment is entirely due to the limited detector resolution. This makes a study of the K_S^0 mass reconstructed from the experimental data a very relevant method for obtaining the resolution of the detector. Furthermore, the other properties of the K_S^0 are also well understood which makes it a suitable tool for studying the features of the detector and the of data reconstruction. The analysis made in this thesis includes the reconstruction of interaction points, the reconstructed mass distributions for K_S^0 decaying inside and outside the target and the estimation of errors from measured kinematic variables.

4.2 Reference system

In the COMPASS reference system the z direction is along the beam, the x direction towards the Jura mountains and the y direction upwards. The upstream target cell extends from $z = -95$ cm to $z = -35$ cm, while the downstream from $z = -25$ cm to $z = 35$ cm, cf Figure 4.

4.3 Good K_S^0 events

4.3.1 Definition of production and decay vertices

Interaction points are called vertices. The point where the reconstructed interaction between the beam muon and the target nucleons takes place is called the *production vertex* or the *primary vertex*. In the primary vertex, hadrons may be produced, and those of interest here are K_S^0 mesons. A point from which two reconstructed oppositely charged tracks originate is called a V^0 *vertex*, and the point where a particle decays is called a *decay vertex*. Decay vertices of neutral particles, such as the K_S^0 meson, are V^0 vertices. Figure 4 shows an interaction with a primary vertex and a V^0 vertex.

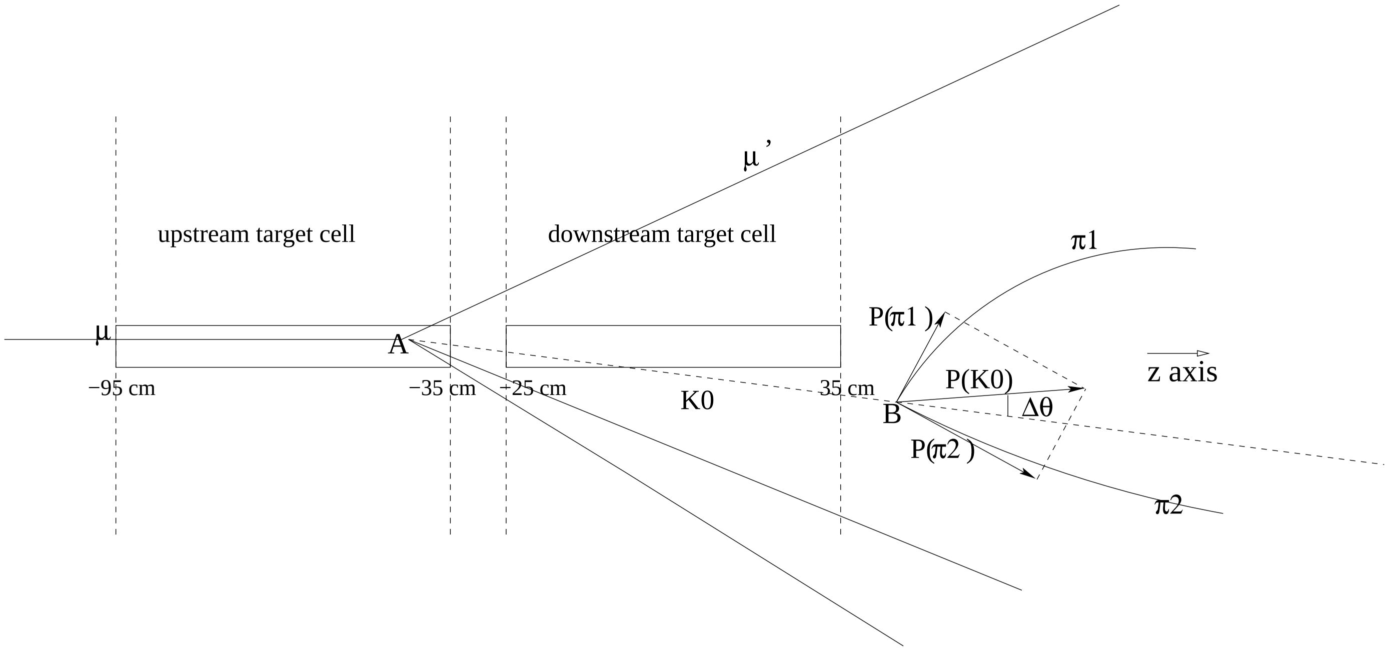

Figure 4: A sketch of a muon interaction within the COMPASS target. A V^0 particle is produced in point A (primary vertex). It decays in point B (decay vertex) into two particles of momenta $P(\pi 1)$ and $P(\pi 2)$. The angle $\Delta\theta$ is defined in the space, see text.

4.3.2 Definition of a good K_S^0 event

Different features of the detectors and of the event reconstruction are studied by analysing so called *good K_S^0 events*. Features of the measured K_S^0 meson such as the *mass resolution* and the *mass shift* of the K_S^0 *mass distribution* are of interest. These are defined as the width and the mean value of a Gaussian curve fitted to the mass distribution, respectively. The mass distribution here is the distribution of the difference between the PDG K_S^0 mass $M_{K_S^0} = (0.49767 \pm 0.000031)$ GeV [9] and the invariant mass of the two charged particles t^+ and t^- in a V^0 vertex:

$$\Delta M(K_S^0) = M(t^+t^-) - M_{K_S^0} \tag{8}$$

A good K_S^0 events is an events that fulfills the following criteria:

- It has a primary vertex with an incoming and a scattered muon reconstructed.
- It has a vertex, situated at least 20 cm downstream the primary one, with two outgoing particles of opposite charge (a V^0 vertex).
- Assuming the two outgoing particles in the V^0 vertex are pions, - $|\Delta M(K_S^0)| < 0.025$ GeV.

The sample of good K_S^0 events is divided into two classes:

1. The z coordinate $z(K_S^0)$ of the K_S^0 decay vertex is well outside the target region, i.e $z(K_S^0) > 56$ cm.
2. The z coordinate $z(K_S^0)$ of the K_S^0 decay vertex is inside the target region, i.e. $z(K_S^0) < 56$ cm.

These two different classes will be studied separately here. In addition to the previous three criteria one more condition must be fulfilled for the event to be a good K_S^0 event. Its tightness depends on the class:

- The angular difference $\Delta\theta$ (see Figure 4) between the momentum vector of the pion-pion system and the line connecting the primary and secondary vertex must be at most 0.04 radians in class 1.
- $\Delta\theta$ must be at most 0.01 radians in class 2.

These criteria will be justified in the following sections.

4.3.3 Motivation for dividing the sample into two classes with respect to decay vertex positions

Most of the V^0 candidates decay inside the target region, as can be seen in Figure 5. The distribution of $\Delta M(K_S^0)$ is cleaner for the case when the V^0

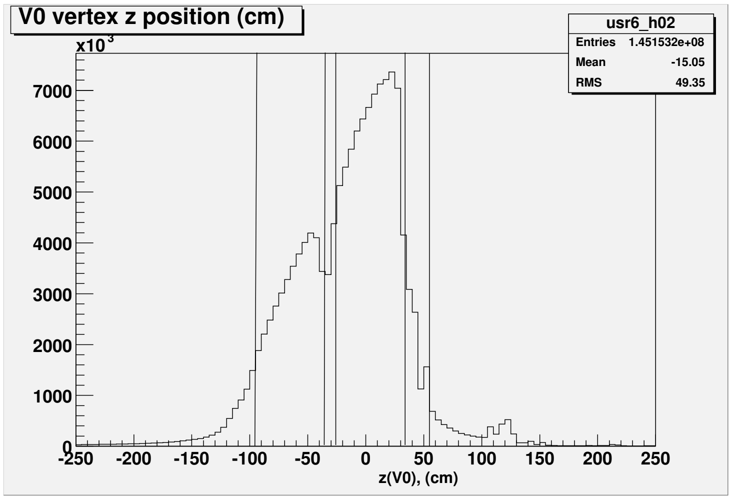

Figure 5: The V^0 vertex distribution for all vertices with two outgoing tracks of opposite charge. The vertical lines mark the target cells and the line $z = 56$ cm that divides the sample into the two classes defined in 4.3.2.

vertex is outside the target than for the case when it is inside, see Figure 6. An important difference between the two classes is that the expected error of the reconstructed mass is much larger inside the target. This is due to multiple Coulomb scattering of the decay products, caused by the large amount of material in the target, the gas mixing chamber and the target containers they have to traverse.

4.3.4 Motivation for requirement on a minimum distance between primary and secondary vertex

The signal to background ratio for the distribution of $\Delta M(K_S^0)$ is improving for larger distances between primary and V^0 vertex for both classes of K_S^0 events (defined in section 4.3.2), see Table 1. In order to achieve a reasonable signal to background ratio without cutting away too many K_S^0 events, a minimum distance cut of 20 cm is applied.

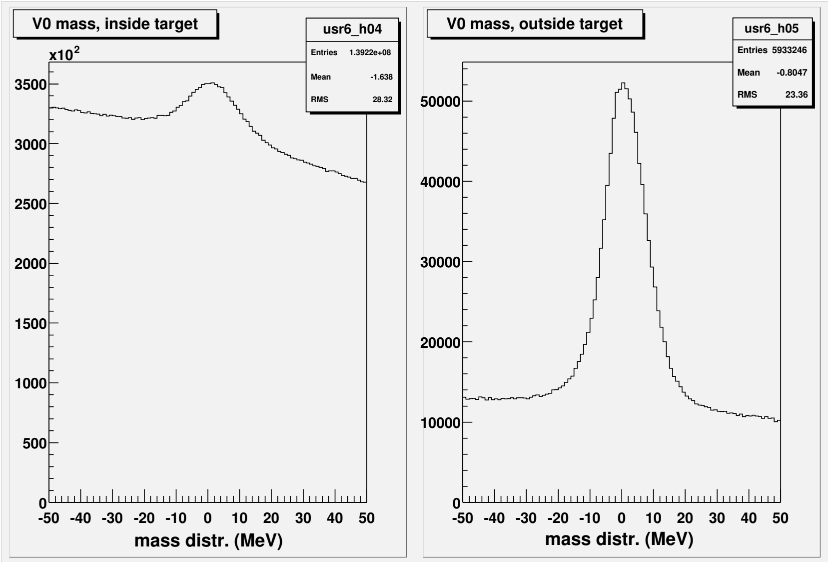

Figure 6: The distribution of the invariant mass of the two outgoing particles in the V^0 vertex, when the V^0 vertex has a z position of $z(V^0) < 56$ cm and $z(V^0) > 56$ cm, respectively.

4.3.5 Motivation for requirement on $\Delta\theta$

Provided the vertex reconstruction is correct, the direction of the momentum vector of the pion-pion system and the vector that connects the primary and the secondary vertex should be identical. Thus the background can be substantially reduced if the angular difference between these vectors must be small. The mass distributions for different cuts on $\Delta\theta$ when the K_S^0 meson decays inside the target region, show that for $\Delta\theta > 0.01$ radians the signal to backgroung ratio is very poor. Since the mass resolution remains constant within errors when the $\Delta\theta$ cut is varied, the sample is not significantly biased by it, see Table 2. From Table 3 it is clear also for class 1, the best signal to background is obtained for $\Delta\theta < 0.01$ radians, but the cut that is applied is $\Delta\theta < 0.04$ radians. That is because a tighter condition would cut away many events that indeed correspond to real K_S^0 events. A large angular difference does not necessarily mean that the reconstructed K_S^0 event does not correspond to a real one, but that it suffers from bad vertex reconstruction.

Table 1: The signal to background ratio S/B for different distances between primary and V^0 vertex d, for K_S^0 candidates decaying inside and outside the target region, respectively

d (cm)	S/B, $z(V^0)$ inside target	S/B $z(V^0)$ outside target
0<d<15	0.05	0.24
15<d<25	0.15	0.86
25<d<35	0.22	1.43
35<d<45	0.27	1.87
45<d<55	0.31	2.03
55<d<65	0.33	2.13
65<d<80	0.36	2.04
80<d<100	0.34	2.06

Table 2: The signal to background ratio S/B and the measured mass resolution σ for events where $z(V^0) < 56$ cm for different values of $\Delta\theta$

$\Delta\theta$ (rad)	S/B	σ (Mev)
$0< \Delta\theta <0.01$	0.75	8.82 ± 0.08
$0.01< \Delta\theta <0.02$	0.22	9.42 ± 0.4
$0.02< \Delta\theta <0.03$	0.08	8.62 ± 0.7
$0.03< \Delta\theta <0.04$	0.07	7.76 ± 1.2
$0.04< \Delta\theta <0.06$	0.07	11.2 ± 2.6
$0.06< \Delta\theta <0.08$	no signal	no signal
$0.08< \Delta\theta <0.1$	no signal	no signal

Table 3: The signal to background ratio S/B and the measured mass resolution σ for events where $z(V^0) > 56$ cm for different values of $\Delta\theta$

$\Delta\theta$ (rad)	S/B	σ (MeV)
0< $\Delta\theta$ <0.01	2.27	6.48 $\pm$ 0.02
0.01< $\Delta\theta$ <0.02	0.69	6.61 $\pm$ 0.1
0.02< $\Delta\theta$ <0.03	0.54	6.39 $\pm$ 0.2
0.03< $\Delta\theta$ <0.04	0.42	6.89 $\pm$ 0.3
0.04< $\Delta\theta$ <0.06	0.31	7.11 $\pm$ 0.3
0.06< $\Delta\theta$ <0.08	0.17	7.13 $\pm$ 0.7
0.08< $\Delta\theta$ <0.1	0.11	6.56 $\pm$ 1.2

4.4 Armenteros plot

An important tool for studying V^0 decays is the Armenteros plot [10], where the relevant variables are the transverse momentum p_t and the asymmetry of the longitudinal momenta p_{asy} of the two decay products. The transverse momentum is independent of the velocity of the decaying particle and it is given by

$$p_t = p_+ sin\phi_+ = p_- sin\phi_- \tag{9}$$

where ϕ_+, ϕ_- are the angles of the decay products with respect to the direction of the V^0 [10]. The longitudinal momentum p_l that is given by

$$p_{li} = p_i cos\phi_i \tag{10}$$

where $i = +, -$ is on the other hand dependent on the velocity of the V^0 and therefore a new variable is introduced, the asymmetry of the longitudinal momenta:

$$p_{asy} = \frac{p_{l+} - p_{l-}}{p_{l+} + p_{l-}} \tag{11}$$

In the Armenteros plot, p_t is plotted versus p_{asy}. K_S^0 events in this plot are distributed along a half-ellipse centered at $p_{asy} = 0$ since p_{asy} has a mean value of

$$\overline{p_{asy}} = \frac{m_+ - m_-}{m_{V^0}} \tag{12}$$

where m_{V^0} is the mass of the V^0 particle. Therefore $\overline{p_{asy}}$ equals 0 for $K^0_S \to \pi^+\pi^-$ decays, and $\Lambda^0 \to p\pi^-$ and $\overline{\Lambda^0} \to \overline{p}\pi^+$ events are distributed along half-ellipses centered at $p_{asy} = 0.69$ and $p_{asy} = -0.69$, respectively. Depending on the emission angle, p_{asy} will fluctuate around its mean value with an amplitude which approaches $2p^*/M_{V^0}$, where p^* is the momentum of the decay products in the K^0_S rest system. For the K^0_S decay, $2p^*/m_{V^0}$ is 0.83 and for Λ^0 and $\overline{\Lambda^0}$ decays it is 0.18. The p_t maximum value for K^0 decays is 206 MeV and for Λ^0 and $\overline{\Lambda^0}$ decays 101 MeV. The Armenteros plot thus shows which type of events a sample consists of. A sample of $K^0_S \to \pi^+\pi^-$ events will also contain $\Lambda^0 \to p\pi^-$ and $\overline{\Lambda^0} \to \overline{p}\pi^+$ since some of the particles that are assumed to be pions are in fact protons or antiprotons. Figure 7 shows an example of an Armenteros plot.

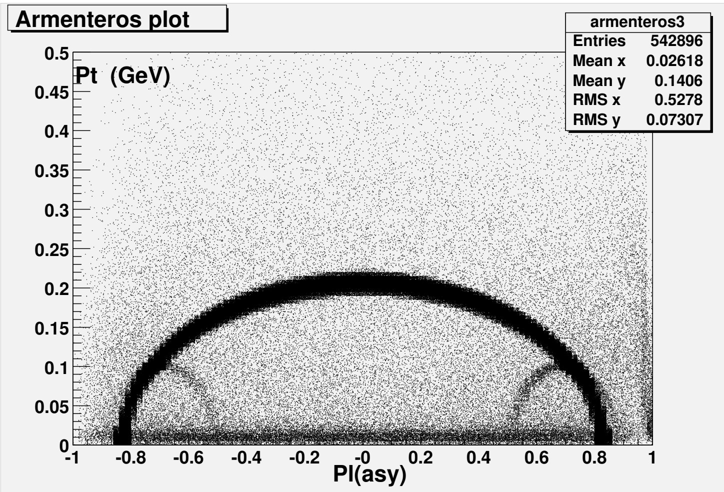

Figure 7: A typical Armenteros plot. The half-ellipse centered at $p_{asy} = 0$ consists of $K^0 \to \pi^+\pi^-$ events, while the half-ellipses to the left and right consist of $\overline{\Lambda} \to \pi^+\overline{p}$ and $\Lambda \to p\pi^-$ events, respectively. The points distributed near $p_t = 0$ mainly correspond to $\gamma \to e^+e^-$ events.

4.5 Software

The software package used in this study is PHAST (PHysics Analysis Software Tool) and is based on C++. The input to PHAST are so called miniDST files prepared by CORAL (the COmpass Reconstruction and AnaLysis program), a system with tools for decoding and reconstruction of events from raw data. CORAL contain among others the package TrafDic that calculates track parameters for each track in each event. In this study, PHAST 5.41 was employed for DST4 data and PHAST 3.16 for DST3 data. Using PHAST, histograms and ntuples are produced and analysed by ROOT.

5 DATA SAMPLE

All the data analysed here were collected in 2002. First, a preliminary study of the DST3 data was performed, where the run periods P1C, P2D and P2F were studied separately for comparison, as well as jointly. At the time of submission of this thesis some data from the DST4 production were available for period P2D. The main part of the results in the following sections come from the DST4 data from period P2D, except the section where differences between run periods are presented. That section will also contain a comparison between the results from DST3 and DST4 data in period P2D. The DST3 data set used here is preselected according to the criteria:

- An event contains one primary vertex.
- An event contains at least one vertex with two outgoing, oppositely charged particles (a V^0 candidate).
- The V^0 vertex is at least 20 cm downstream of the primary one.
- The invariant mass of the two outgoing particles in the V^0 vertex differs from the K_S^0 mass $M_{K_S^0}$ with at most 0.1 GeV.

The sample of DST4 data being used is preselected so that:

- Each event contains a V^0 vertex.
- The invariant mass of the two outgoing particles in the V^0 vertex differs from the K_S^0 mass $M_{K_S^0}$ with at most 0.1 GeV.

This preselected sample is used for all studies except the estimation of the K_S^0 yield. There, the number of good K_S^0 events is normalised to the total number of events in the miniDST files. An event in a miniDST file is defined as one with at least one vertex in it, that not necessarily has to be a primary one. The preselection does not affect the compared results.

The background consists of events with false V^0 vertices due to faulty vertex reconstruction, of $\gamma \rightarrow e^+e^-$ events and of Λ baryons.

The plots shown in this paper are made using different criteria that are specified each time, but also using different samples. Therefore, the number of entries shown is not an estimate of the efficiency of the cuts.

6 RESULTS

Among the total number of events in the DST4 data, 0.46 % contain good K_S^0 candidates. Among the total number of events with a μN interaction, defined as an event containing a primary vertex, the relative number of good K_S^0 candidates is 2.8 %.

6.1 Vertex distributions

6.1.1 Primary and V^0 vertex distributions

The distributions of primary vertices as well as V^0 vertices in the z direction need to be studied for a deeper understanding of how the target, the materials around the target and the materials in the detector planes affect the interactions. The distributions of all primary vertices and all V^0 vertices

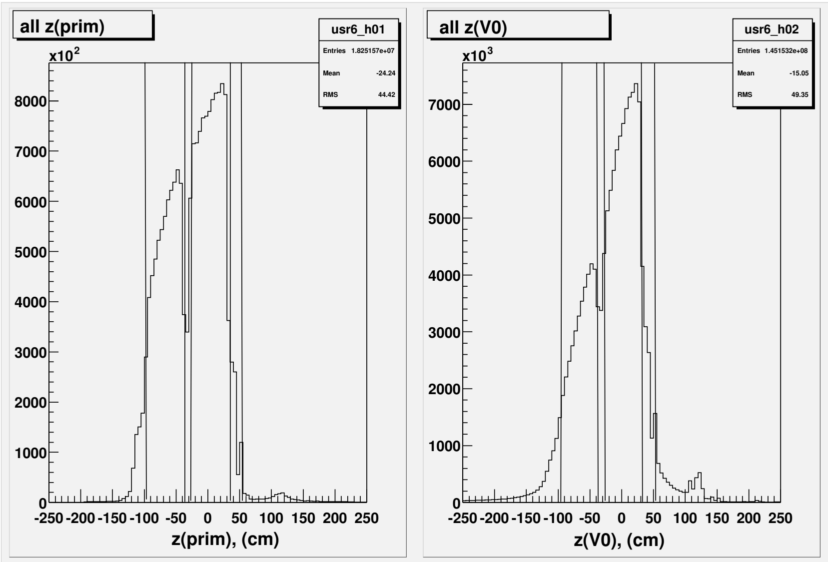

Figure 8: Left: The z distribution of all primary vertices in the sample. Right: The z distribution of all vertices with two outgoing, oppositely charged particles . The vertical lines mark the two target cells except rightmost one, marking the point z = 56 cm.

in the sample have similar shapes as can be seen in Figure 8. This leads to a suspicion that many V^0 vertices are primary vertices with two outgoing, oppositely charged particles, whereof one can be the scattered muon. A demand of a minimum distance between the primary and the V^0 vertex reduces substantially the amount of V^0 vertices (see Figure 9), which confirms the

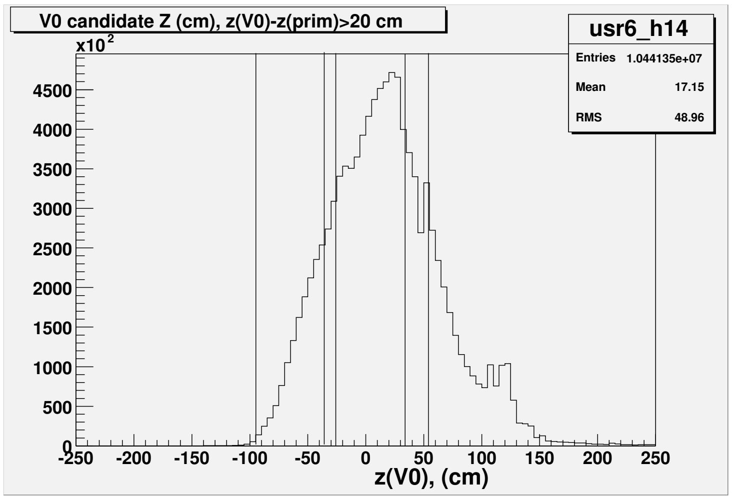

Figure 9: This picture shows the distribution of V^0 vertices after requiring the V^0 vertex to be 20 cm downstream of the primary one. The vertical lines mark the target cells except the rightmost one, marking the z = 56 cm point.

suspicion. The distribution of primary vertices in good K_S^0 events along with the distribution of good K_S^0 decay vertices are shown in Figure 10. It is clear that more measured K_S^0 mesons are produced in the downstream target cell than in the upstream. This is partly due to the acceptance of the target polarising magnet, since the K_S^0 mesons can undergo nuclear reactions within the magnet so that the event is lost.

Figure 11 shows the mass distribution for K_S^0 mesons produced in the upstream and downstream target cell, respectively. Table 4 show the mass shift Δm and the mass resolution σ for the K_S^0 mesons produced in the upstream and downstream target cell, respectively. The amount of good K_S^0 events with production vertex in the upstream and downstream target cells is also given. The measured K_S^0 mesons that are not produced in any of the target cells are produced within the material in the target container, the gas mixing chamber, the target windows and the detector planes.

6.1.2 A now solved problem in the vertex reconstruction

The primary vertex distribution for $z(prim) > 56$ cm (outside the target region) in DST3 data, was not smooth but consisted of several peaks, see Figure 12. Most of these peaks are centered at a z-coordinate that coincide with detector planes or windows in the target container (marked in the figure). The material in the detector planes acts as auxiliary targets. Two peaks, however, appear where there is no material present, at $z \approx 160$ cm

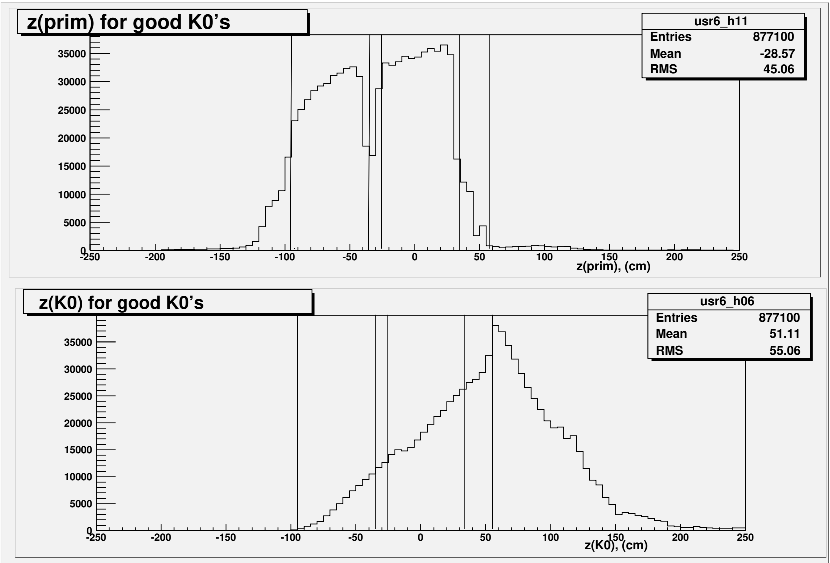

Figure 10: Left: The primary vertex distribution for good K_S^0 events. Right: The K_S^0 decay vertex distribution. The two target cells are marked with vertical lines, and the line at z = 56 cm, marks the cut that divides the K_S^0 events into two classes, defined in section 4.3.2. This cut causes the apparent discontinuity in the distribution at that piont.

Table 4: The mass shift Δm, the mass resoltion σ and the relative amount of the good K_S^0 events that have primary vertex in upstream and downstream target cell, respectively

Quantity	upstream cell	downstream cell
Δm, (MeV)	1.54 $\pm$ 0.04	1.59 $\pm$ 0.02
σ, (MeV)	7.39 $\pm$ 0.05	6.77 $\pm$ 0.02
K_S^0 yield in cell (%)	28	49

and $z \approx 173$ cm. A further investigation showed that the two peaks appear only for primary vertices where there is one outgoing particle only, namely the scattered muon, and that they appear only for very small scattering angles, as illustrated in Figure 13. Events with only one outgoing particle were divided into two cases:

1. Events with primary vertices in the region $155 < z < 180$ cm

2. Events with primary vertices outside this region

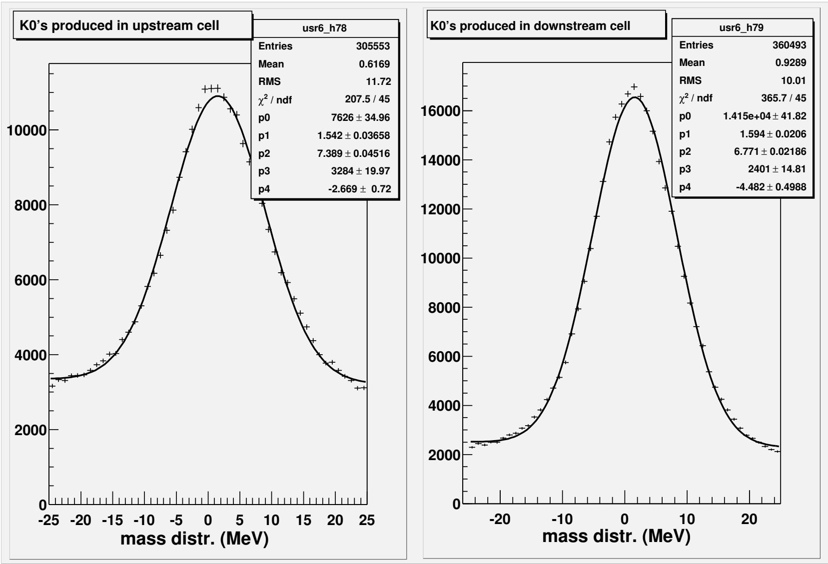

Figure 11: The reconstructed invariant mass distribution of K_S^0 mesons produced in the upstream and downstream target cell, respectively. The curves show the fitted functions, i.e. Gaussian curves and linear backgrounds. The fit parameters are given in the inserts.

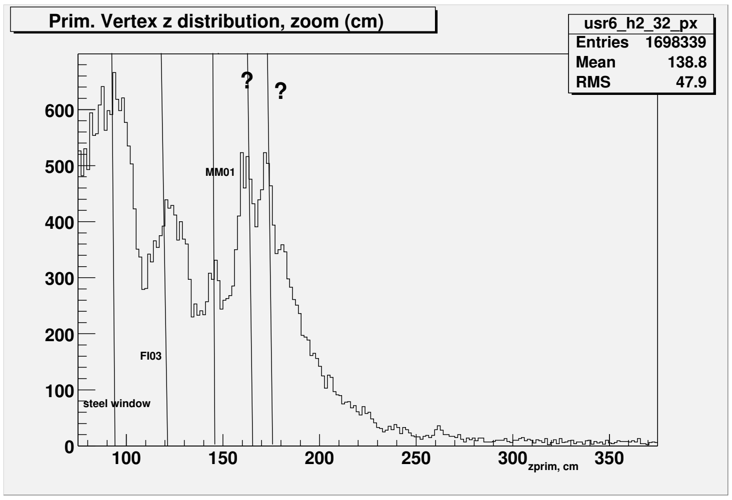

Figure 12: A zoom of the primary vertex distribution with DST3 data from period P2D. Detector planes that coincide with peaks are marked. Two peaks, marked with '?' do not correspond to any detector planes.

As can be seen in Figure 14, the momentum of the scattered muon for case 1 is generally lower than for case 2. Moreover, the first point where the

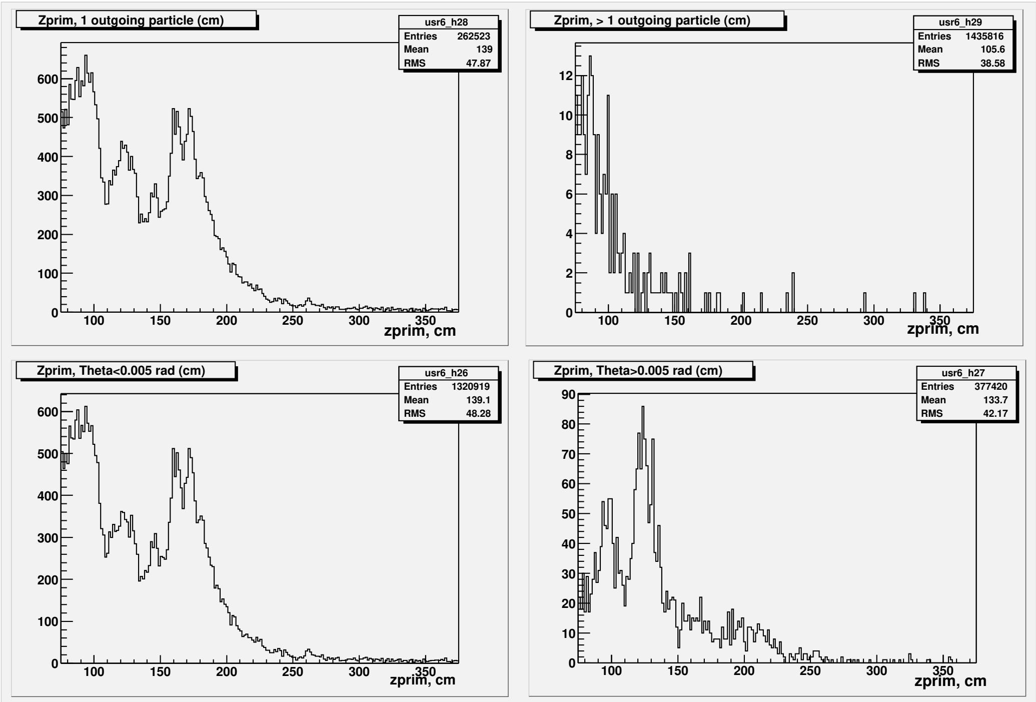

Figure 13: The two pictures on the top show the (zoom of the) primary vertex distribution for only one outgoing particle (the scattered muon) and with more than one outgoing particle in the vertex, respectively. In the bottom the (zoom of the) primary vertex distribution is shown for small and large scattering angles, respectively.

track of the scattered muon is registered, called the *first measured point*, is in case 1 generally upstream of the vertex, i.e. the point where the muon is scattered. In case 1, the first measured point is also very confined in the radial direction compared to case 2. This points towards that what is registered in the first measured point is actually the beam muon, misidentified as the scattered muon. An event-by-event investigation [11] showed that the primary interaction actually takes place within and downstream of the RICH detector, but the hits produced in the LAS by the incoming muon are misinterpreted as hits produced by the scattered one. Thus the track of the scattered muon is very poorly reconstructed and the vertex is assigned a false position. This observation has lead to changes in the reconstruction procedure [11] and in the current version of DST, the peaks in the vertex distribution at $z = 160$ cm and at $z = 173$ cm are almost absent, see Figure 15.

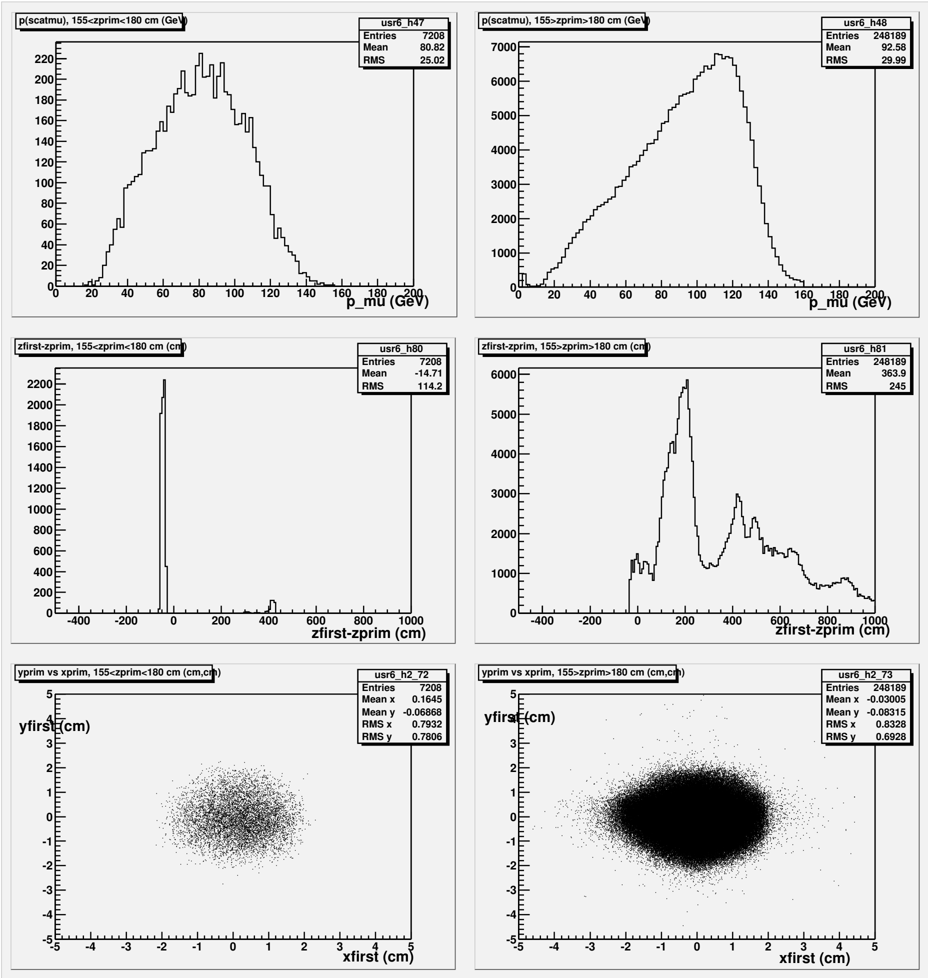

Figure 14: Top: The momentum distribution of the scatterd muon for case 1 and 2 defined in the text, respectively. Middle: The difference between the z position of the first measured point of the muon track and the vertex illustrates that in case 1, the vertex is downstream of the first measured point. Bottom: The x and y coordinates of the first measured points for the two cases.

6.1.3 Distance between primary and K_S^0 vertex in the rest system of the K_S^0

A study of the distance between the primary and the decay vertex of the K_S^0 in the K_S^0 rest system provides an independent test of how many of the

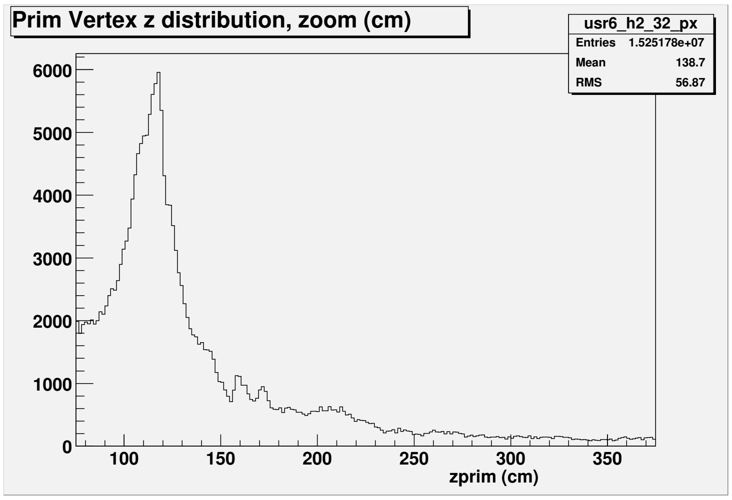

Figure 15: The primary vertex distribution after changes in the reconstruction procedure [11].

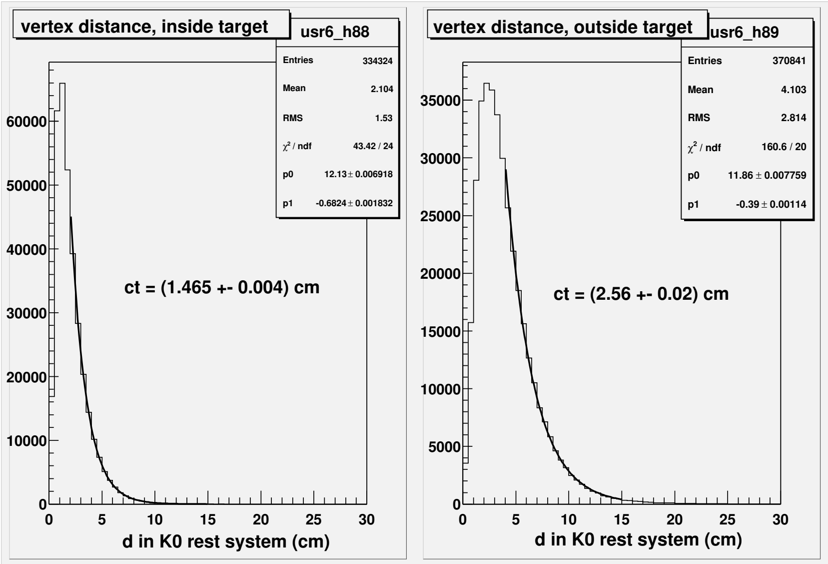

Figure 16: The distance between primary and seconday vertex in the K_S^0 rest system for K_S^0 mesons decaying inside and outside the target, respectively.

K_S^0 candidates that actually are K_S^0 events. In Figure 16 this distance is shown, fitted to an exponential function ($p^0 \cdot e^{-p^1 \cdot d}$, where p^0 and p^1 are fit parameters) for K_S^0 mesons decaying inside and outside the target. The factor in the exponent $(-p^1)$ is the reciprocal of $c\tau$, i.e. from the fit parameter the lifetime of the K_S^0 can be calculated. The K_S^0 that decay outside the target are found to reproduce the PDG value $c\tau = 2.679$ cm [9] fairly well: $c\tau = (2.56 \pm 0.02)$ cm, if a tighter mass cut of $|\Delta M_{K^0}| < 0.015$ GeV is applied, while the K_S^0 mesons decaying inside the target give a false numerical value: $c\tau = (1.465 \pm 0.004)$ cm . The sample of K_S^0 events with decay vertex inside the target thus contains more background than the sample with decay vertex outside, as will be confirmed later.

6.2 K_S^0 mesons decaying outside the target region

The total sample of good K_S^0 events contains 58 % of K_S^0 events with decay vertex outside the target region.

6.2.1 Mass distributions

The mass resolution, the mass shift and the signal to background ratio can be retrieved from fit parameters of the reconstructed mass distribution ΔM_{K^0}. The mass resolution and the mass shift is studied separately for two different cases, namely when both pion tracks from the K_S^0 decay end in the LAS and when both tracks end in the SAS. Results from DST3 data show that mass shift, mass resolution and signal to backround ratio vary depending on from which run period the data come. When this study was made, DST4 was only available for the period P2D, so to show how the mentioned quantities vary, results from DST3 data are used. Since the class of K_S^0 mesons that decay outside the target gives clean mass distributions, the study is limited to this class. To get a first estimate of how results may change when DST4 data are used, the DST4 results for period P2D are included in the study for a comparison. It is found that the mass shift in LAS is large and positive for the periods P2D and P2F, while it is smaller and negative in period P1C. For the SAS, the mass shift is, within errors, the same in all three run periods. The mass resolution in P1C is a little worse than in P2D and P2F. The signal to background ratio is, however, better in P1C. In that period, the drift chambers did not operate. The results are summarised in Table 5. A comparison of the results from DST3 data and DST4 data shows that the mass resolution in LAS is better and the mass shift is smaller for the DST4 data compared to DST3. In SAS, the results are within errors almost unchanged. The mass shift in the LAS may be due to an overlap between the magnetic fields of the target solenoid and the spectrometer magnet SM1, so that the total field is shifted. That would lead to a false estimation of the pion momentum, which in turn causes the mass shift. The signal to background ratio is improved for DST4 compared to DST3 data.

Table 5: Mass shift Δm and mass resolution σ for the cases when both pion tracks from the K_S^0 decay end in the LAS and the SAS, respectively, and the signal to background ratio S/B for tracks ending anywhere in the spectrometer. All K_S^0 mesons in this study decay outside the target region.

Quantity	P1C (DST3)	P2D (DST3)	P2F (DST3)	P2D (DST4)
Δm, LAS (MeV)	-1.10 $\pm$ 0.08	4.68 $\pm$ 0.04	4.63 $\pm$ 0.06	2.80 $\pm$ 0.03
Δm, SAS (MeV)	-1.61 $\pm$ 0.14	-1.55 $\pm$ 0.05	-1.58 $\pm$ 0.07	-1.65 $\pm$ 0.03
σ, LAS (MeV)	7.32 $\pm$ 0.09	7.24 $\pm$ 0.05	7.18 $\pm$ 0.08	6.12 $\pm$ 0.04
σ, SAS (MeV)	5.93 $\pm$ 0.2	4.98 $\pm$ 0.07	4.81 $\pm$ 0.1	5.08 $\pm$ 0.05
S/B	2.51	1.60	1.59	1.76

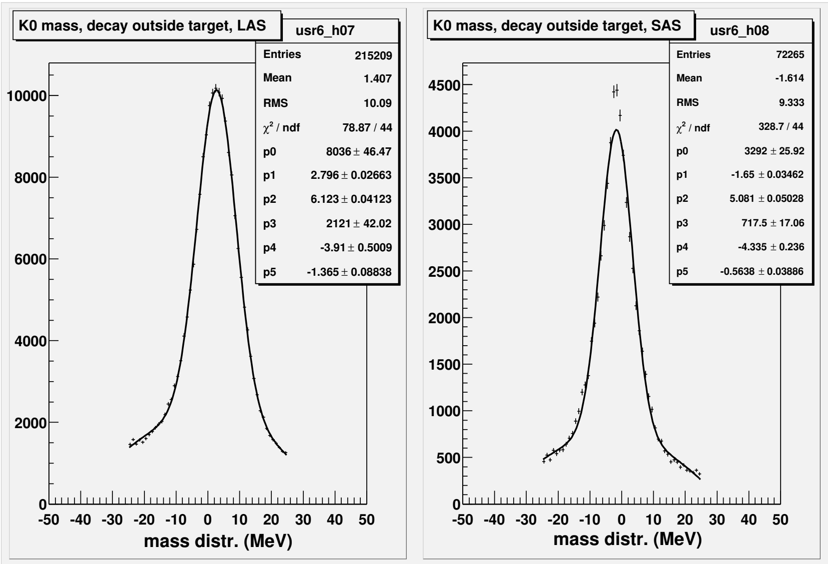

Figure 17: The fitted mass distributions from LAS and SAS, respectively. The curves show the fitted functions, i.e Gaussian curves and second degree polynomial backgrounds. The fit parameters are given in the inserts.

Figure 17 shows the fitted mass distributions for data from period P2D in DST4. There one can see that χ^2 per degree of freedom is very bad for the fit in the case when the pion tracks end in the SAS, $\chi^2/d.o.f = 328.7/44$. To understand this, the subsample of K_S^0 decaying outside the target and with pion tracks ending in the SAS was investigated further. It was found that for a very particular class of K_S^0 events, a very peculiar mass distribution is obtained. This class consists of events where

- the K_S^0 mesons decay within or downstream of the SM1
- the tracks of the pions from the decay have their first measured point in one of the GM detector planes
- the pions from the decay traverse a mass equivalent to > 1.0 radiation length

The mass distribution of this class can be seen in Figure 18. The best fit is obtained when the distribution is fitted to two Gaussian curves and a linear background, i.e there are two samples of K_S^0. One sample has a very good mass resolution $\sigma_1 = (2.30 \pm 0.09)$ MeV and a small negative shift $\Delta m_1 = (-2.01 \pm 0.06)$ MeV, and the other sample has a worse mass resolution $\sigma_2 = (6.43 \pm 0.2)$ MeV and a large negative shift $\Delta m_2 = (-3.98 \pm 0.1)$ MeV. Why these two samples occur is not yet completely understood. It seems the sample of K_S^0 events giving the narrow distribution consists of events where the decay pions hit GM detectors only, and their tracks would then be very well measured and have small errors since the resolution in the GM detectors is better than in the other types of detectors. This sample of events is likely to be the reason why it is so difficult to make a good fit to one Gaussian for the subclass of K_S^0 with tracks ending in the SAS.

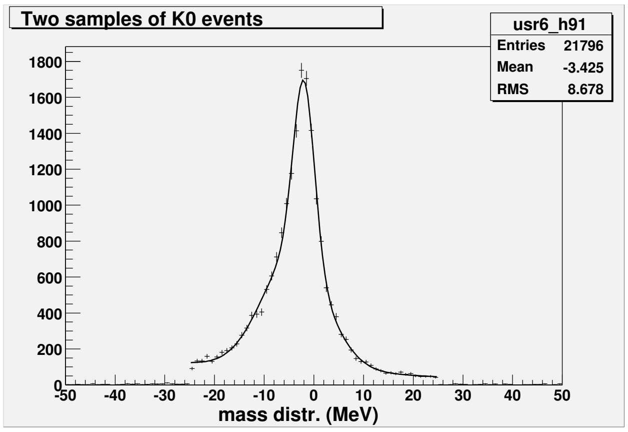

Figure 18: The subsample of K_S^0 events defined in the text. The curve shows the fitted fuction: two Gaussian curves and a linear background.

6.2.2 Armenteros plot

In Figure 19 the Armenteros plot for K_S^0 mesons decaying outside the target is shown. The preselection criterium $|\Delta M(K_S^0)| < 0.1$ GeV gives the wide band around the K_S^0 half-ellipse. The sample contains $\gamma \rightarrow e^+e^-$, $\Lambda \rightarrow p\pi^-$ and $\overline{\Lambda} \rightarrow \overline{p}\pi^+$ events as can be seen in the figure.

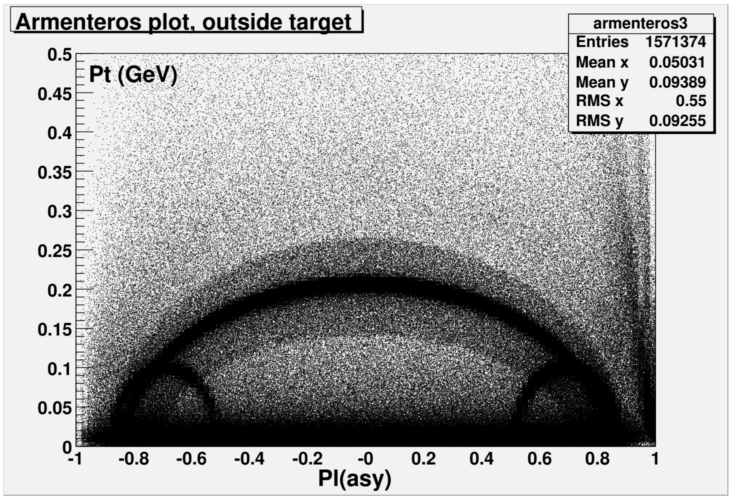

Figure 19: The Armenteros plot for K_S^0 mesons decaying outside the target. No mass cut is applied except for the one in the preselection, see section 5.

6.2.3 K_S^0 mass resolution calculated from TrafDic errors

The error of the invariant mass of the pion-pion system for each event can be calculated from the errors in the track parameters (momentum, angle and position) obtained from TrafDic. Here we follow the method of [12]. The invariant mass of the system is given by

$$M_{K_S^0}^2 = 2M_\pi^2 + 2E_{\pi^+}E_{\pi^-} - 2p_{\pi^+}p_{\pi^-}cos\theta_{\pi^+\pi^-} \tag{13}$$

where $\theta_{\pi^+\pi^-}$ is the $\pi^+\pi^-$ opening angle. The error of the mass is:

$$\begin{aligned}(\delta M)^2 &= \sum_{i=\pi^+,\pi^-}(\frac{\partial M}{\partial p_i}\delta p_i)^2 + 2\sum_{i=\pi^+,\pi^-}\frac{\partial M}{\partial p_i}\frac{\partial M}{\partial cos\theta_{\pi^+,\pi^-}}cov(p_i, cos\theta_{\pi^+,\pi^-}) \\ &+ \left(\frac{\partial M}{\partial cos\theta_{\pi^+,\pi^-}}\delta cos\theta_{\pi^+,\pi^-}\right)^2\end{aligned} \tag{14}$$

assuming $cov(p_{\pi^+}p_{\pi^-}) = 0$. The errors of the pion momenta, the opening angle $\theta_{\pi^+\pi^-}$ and the covariance can be calculated from the errors of the track parameters at the decay vertex: dp, dx, dy, ddx, ddy, from TrafDic in the way described in [12]. In this way, the error in the invariant mass can be divided into contributions from the momentum error

$$\text{dmp} = \frac{1}{2M}\sqrt{\sum_{i=\pi^+,\pi^-}(\frac{\partial M}{\partial p_i}\delta p_i)^2} \tag{15}$$

from the error in the opening angle

$$\text{dmcos} = \frac{1}{2M}(\frac{\partial M}{\partial cos\theta_{\pi^+,\pi^-}}\delta cos\theta_{\pi^+,\pi^-}) \tag{16}$$

from and their covariance

$$\text{dmcov} = \frac{1}{2M}\sqrt{2\sum_{i=\pi^+,\pi^-}\frac{\partial M}{\partial p_i}\frac{\partial M}{\partial cos\theta_{\pi^+,\pi^-}}cov(p_i, cos\theta_{\pi^+,\pi^-})} \tag{17}$$

The contributions were studied separately and the sum was compared to the measured mass resolution. From Figure 20 it is clear that on average, the contribution from the covariance is neglible compared to the contributions from the momenta and the opening angle, that are of the same order. Thus, the contribution from the covariance will be neglected from now on. In Figure 21, where the momentum error $\delta p/p$ is plotted versus the momentum, a clear band structure appears. A similar band structure is present when the contribution from the momentum error dmp is plotted *versus* the momentum of one of the pions, see Figure 21. The band structure is not as distinct as in the case of the momentum error $\delta p/p$ only, but a comparison should be done with caution since the quantity dmp depends on the momentum error of both decay pions while $\delta p/p$ depends on one of the pions. Figure 22, where the momentum error $\delta p/p$ is shown for different groups of detector planes where the pion track ends, shows that the bands in Figure 21 correspond to different detector planes.

The events can be divided into two subsamples with respect to the magnitude of dmcos:

1. dmcos $<$ 1.3 MeV
2. dmcos $>$ 1.3 MeV

since Figure 23 shows a minimum in the point density between dmcos $\approx$ 1.0 MeV and dmcos $\approx$ 1.5 MeV. The first subsample contains mainly back-

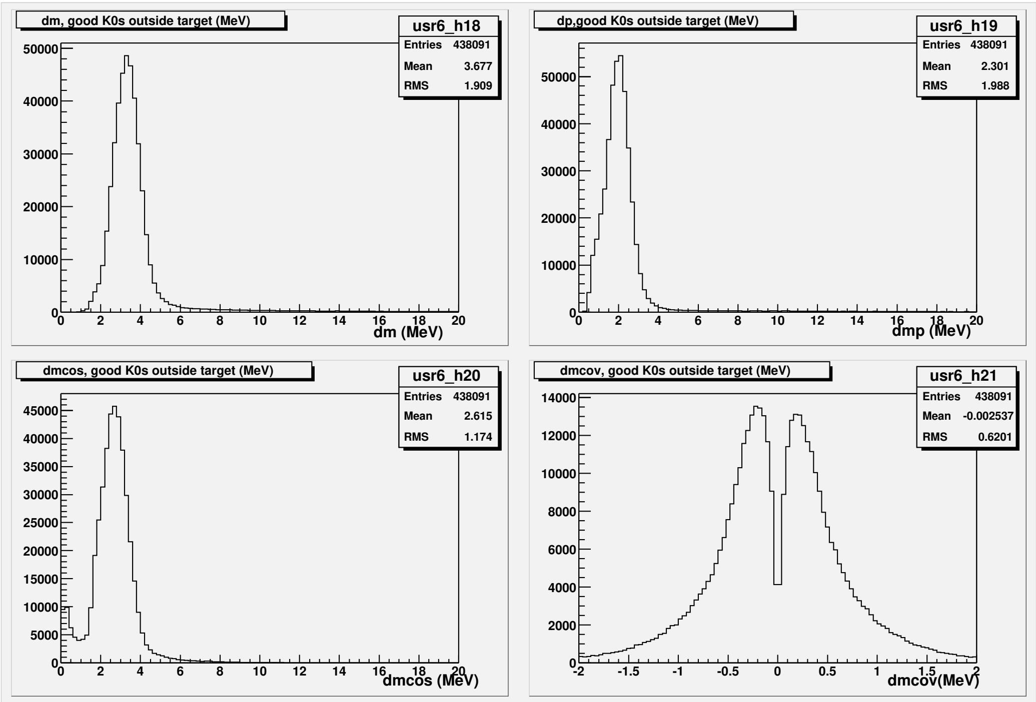

Figure 20: Top left: The total mass error calculated from track parameters. Top right: The contributions from the momentum error. Bottom left: The contribution from the error in the opening angle. Bottom right: The contribution from the covariance of the momentum and the opening angle.

ground. The fact that the events in the first subsample generally have very small p_t, as can be seen from the Armenteros plot in 24, suggests that these events are in a large extent photons producing e^+e^- pairs. From the Armenteros plot it is also concluded that the subsample contains manyΛ baryons. The mass distribution of the first subsample confirms that it is mainly background. The second subsample does contain a clean sample of good K_S^0 events. This can be seen from the mass distribution in Figure 24, which gives a distinct peak. The Armenteros plot show a higher point density around the K_S^0 half-ellipse mentioned in section 4.4 as expected when the sample to a large extent consists of good K_S^0 events.
Figure 25 illustrates how the contribution from the opening angle error to the total mass error depends on in which group of detector planes the pion tracks end.

The total mass error dm, that contains contributions from dmp and -

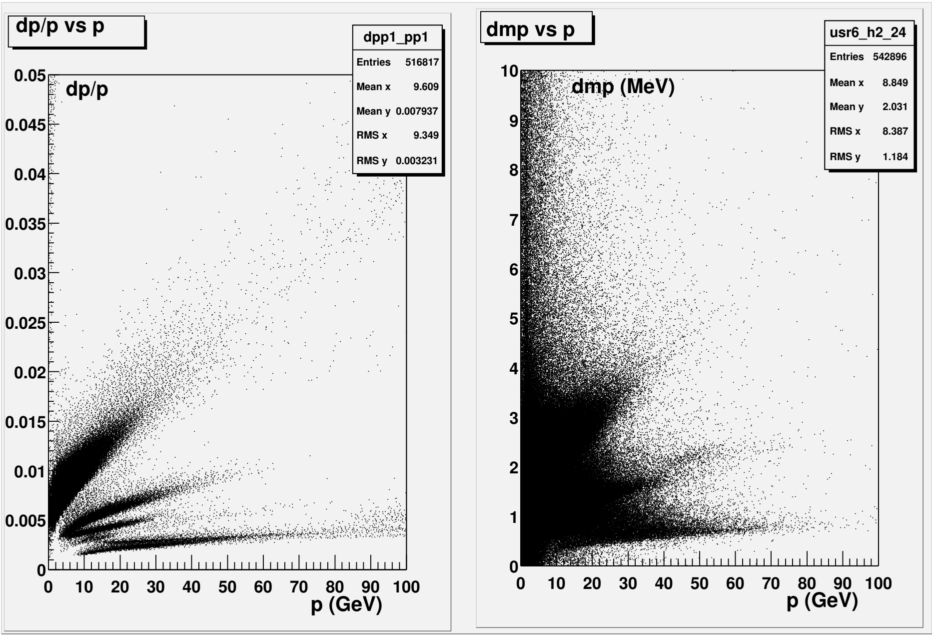

Figure 21: Left: The relative error in the momentum of one of the pions from the K^0_S decay over the momentum $\delta p/p$ is plotted *versus* the momentum of the pion. The bands are related to different detector planes where the pion track ends. To the right the contribution to the mass error from the momentum error of both pions is plotted *versus* the momentum of one of the pions.

dmcos, also varies depending on in which group of detector the pion tracks end. Here, the mass error is defined as the mean value of the dm distribution. In Table 6 it is compared to the measured mass resolution, i.e. to the σ of the mass distribution obtained for tracks ending in different groups of detector planes. The calculated mass error is clearly smaller than the measured mass resolution, and while the calculated errors are increasing the further downstream in the spectrometer the tracks end, the measured resolution generally gets better. The best measured resolution is obtained for tracks ending in FI07 and HO03, i.e. tracks that have crossed most of the GM planes. The fact that the measured mass resolution is improved for tracks ending further downstream in the spectrometer is not surprising since these tracks are likely to be registered in many detector planes so that their tracks, and therefore also their momenta, are well measured. The mass error calculated from the track parameters apparently does not reproduce this, which means that the method of estimating the track parameters needs to be investigated.

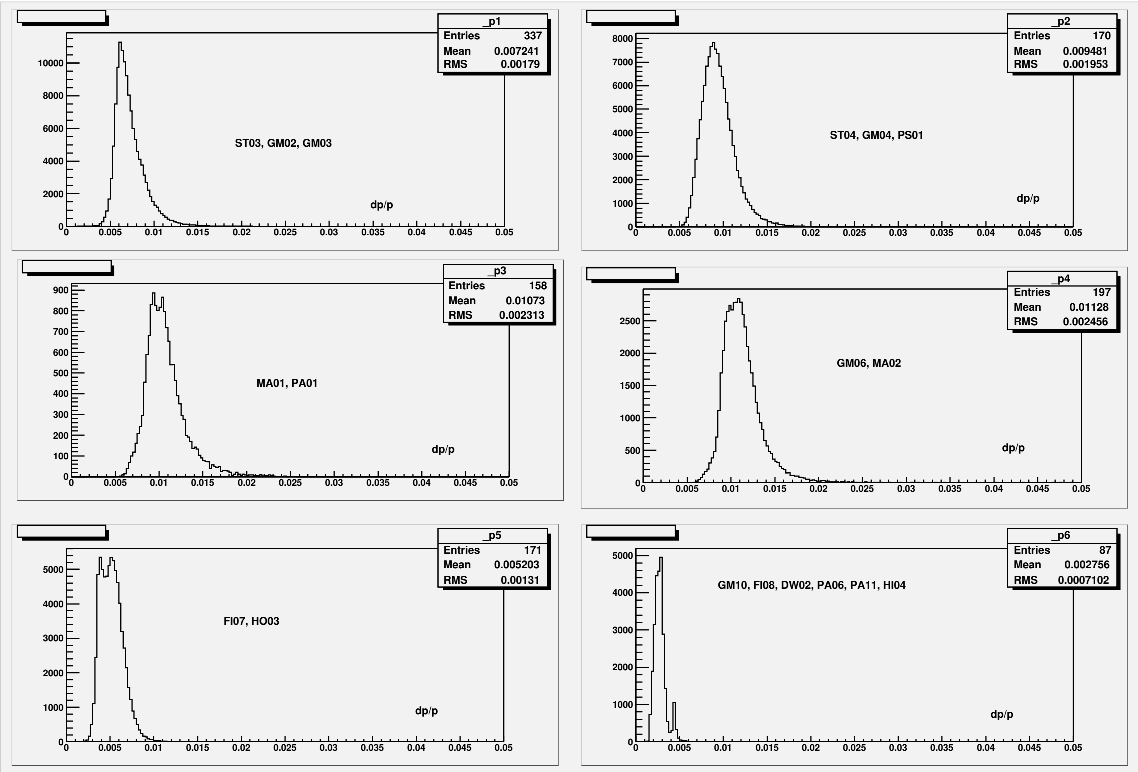

Figure 22: The momentum error for one of the pions from the K_S^0 decay over the momentum of the pion $\delta p_\pi / p_\pi$ for different detector planes where the pion track ends. The two pictures in the bottom both correspond to events where the tracks end in the SAS.

6.3 K_S^0 mesons decaying inside the target region

The total sample of good K_S^0 events contains 42 % K_S^0 mesons decaying within the target region.

6.3.1 Mass distribution

The region inside the target is in turn divided into different subregions. This class of K_S^0 candidates is further divided into smaller subclasses depending in which of these different regions the K_S^0 candidate decays. Radially, three regions are defined:

- i: This region consists of the two target cells. When the V^0 vertices are

Table 6: The mass error calculated from track parameters defined as the mean value of the dm distribution, the RMS value for the dm distribution, the measured mass resolution σ and the mass shift Δm for different groups of detector planes where the pion tracks end. At the bottom of the table, these quantities are shown for the whole sample of K_S^0 mesons decaying outside the target.

Detector planes	dm mean (MeV)	dm RMS (MeV)	σ (MeV)	Δm (MeV)
ST03, GM02, GM03	2.99	0.7	6.99 ± 0.07	2.73 ± 0.06
ST04, GM04, PS01	3.49	0.5	6.42 ± 0.04	2.96 ± 0.04
MA01, PA01	3.90	0.6	5.08 ± 0.4	2.54 ± 0.3
GM06, MA02	4.13	0.6	6.37 ± 0.1	1.84 ± 0.1
FI07, HO03	3.91	1.0	3.57 ± 0.1	-2.49 ± 0.07
GM10, FI08, DW02, PA06, PA11, HI04	4.04	1.0	4.62 ± 0.2	-1.88 ± 0.2
Total sample	3.68	1.0	6.02 ± 0.03	1.26 ± 0.02

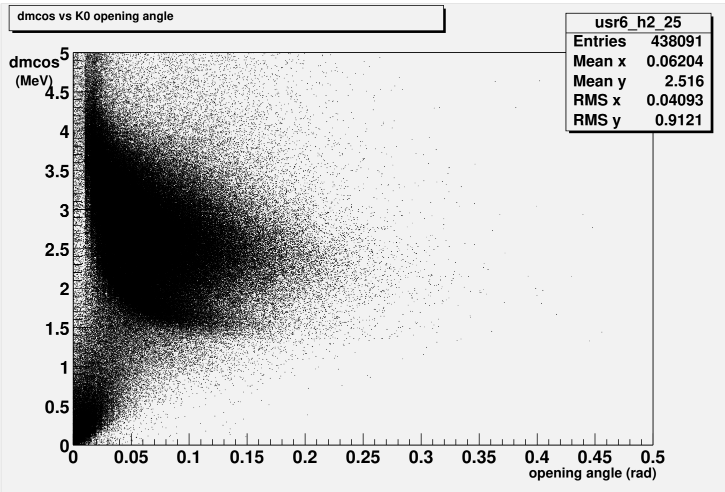

Figure 23: The contribution from the error in the K_S^0 opening angle to the total mass error *versus* the opening angle.

inside this region the signal to background ratio is the worst. That is because most tracks originate from the target cells so the probability to have faked V^0 vertices is large. Moreover, errors on the track parame-

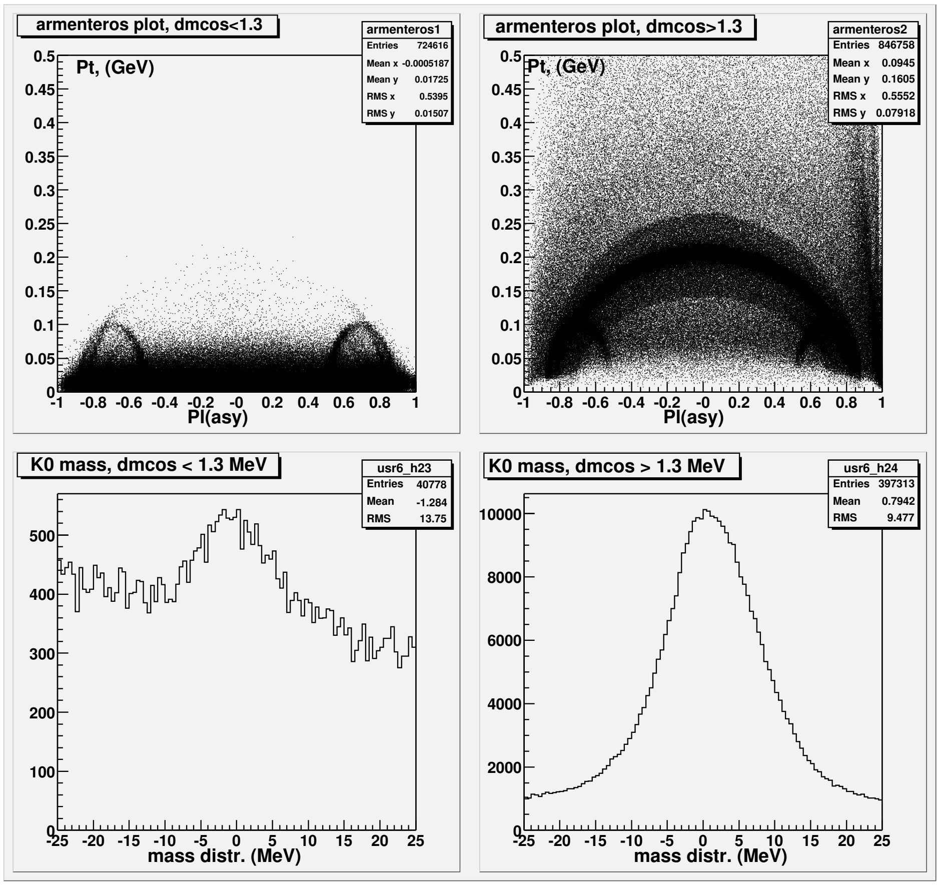

Figure 24: Top: The Armenteros plot for the case dmcos < 1.3 MeV and dmcos $>$ 1.3 MeV, respectively. No mass cut is applied except for the one in the preselection (see section 5). Bottom: The respective mass distributions.

ters are larger than in the other regions because of multiple Coulomb scattering in the target material. The signal to background ratio is better for K^0_S decaying in the downstream than in the upstream target cell as shown in Figure 26 and Table 7. Also the mass resolution is better for the downstream cell, as expected, since the pions from the decay in the downstream cell have less material to traverse than those that decay in the upstream. The mass shift is smaller in the upstream than in the downstream target cell. Of the whole sample of good K^0_S events, 10 % decay within one of the target cells. Of those K^0_S mesons, 13% decay in the upstream cell and 87% in the downstream. This is partly due to the distance cut between primary and secondary vertex, partly due to the acceptance of the target solenoid and also due to the relatively long lifetime of the K^0_S meson.

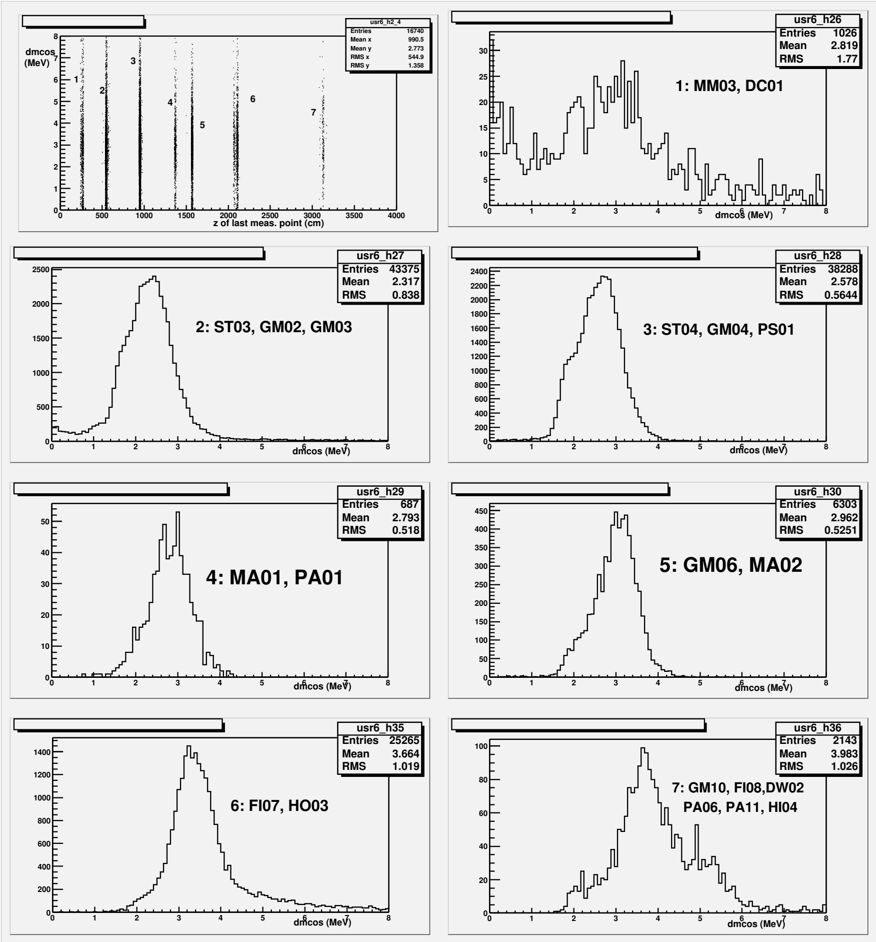

Figure 25: Top left:The z coordinate of the last measured point for both pion tracks from the K_S^0 decay. The other pictures show the contribution from the error in the K_S^0 opening angle to the total mass error dmcos for different detector planes in the LAS where both pion tracks from the K_S^0 decay end. Bottom: Events where the pion tracks end in detector planes the SAS.

The target cells can also be studied in slices in the z direction. The further downstream in the target the K_S^0 meson decays, the larger the signal, as seen in Figure 27. The background in the upstream cell increases a little as the vertex z position moves downstream, but in the downstream target cell, the background is fairly constant.

- ii: This region is located between the target and the target container. The pions from the K_S^0 mesons that decay here still undergo multiple Coulomb scattering in the helium within the container, or the material of the container. The pion tracks might also traverse a part of the target and get scattered.

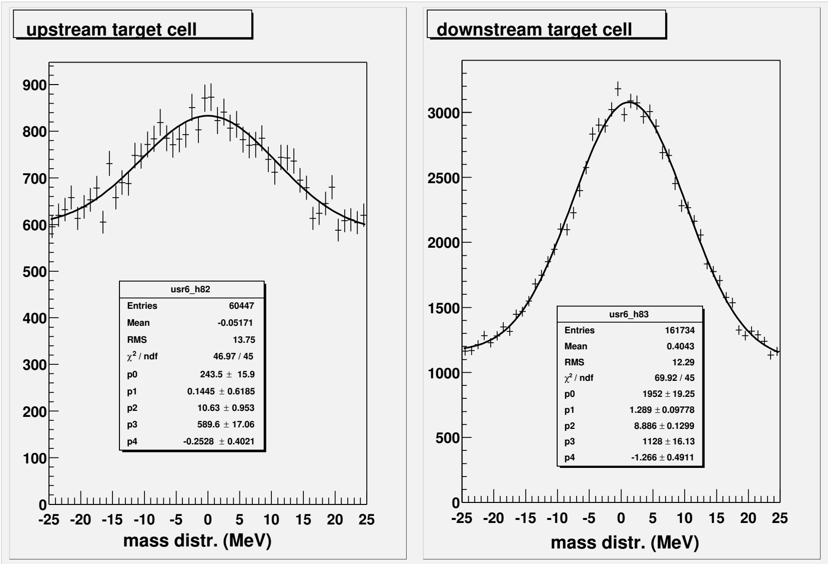

Figure 26: The mass distribution for K_S^0 mesons decaying within the upstream and downstream target cells, respectively. The curves are the fitted functions, i.e Gaussian curves and linear backgrounds.

Table 7: The signal to background ratio S/B, the mass resolution σ and the mass shift Δm for the upstream and downstream target cell, respectively

Quantity	Upstream target cell	Downstream target cell
S/B	0.22	0.77
σ (MeV)	10.63 ± 1.0	8.89 ± 0.1
Δm (MeV)	0.14 ± 0.6	1.29 ± 0.1

- iii: This region lies outside the target container. When the K_S^0 decay vertex is in this region, the pion tracks that traverse the material in the target container or the target itself undergo multiple Coulomb scattering.

As the vertex position is moved away radially from the target center the probability of the pion tracks traversing a large amount of the target and target container material decreases. Since more tracks originate from the very target the probability of having faked V^0 vertices also decreases, and we expect the signal to background ratio as well as the reconstructed mass resolution to improve as the vertex position is moved outwards. This is

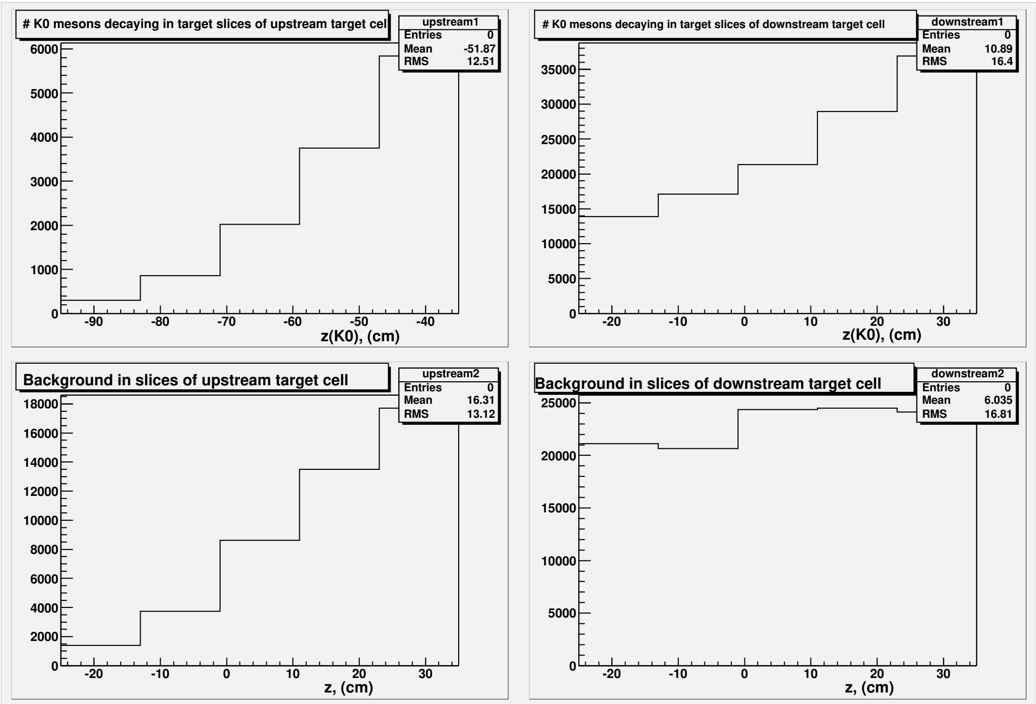

Figure 27: Top: The number of K_S^0 decaying in different slices in the upstream and downstream target cell, respectively. Bottom: The number of background events in each slice.

indeed observed as can be seen from Figure 28 and Table 8. The K_S^0 mass shift is smaller the further inwards in the target the decay vertex is, i.e. the more matter the pions have to traverse. Having in mind the result from the comparison of the two target cells, where the shift in the upstream target cell was smaller than in the downstream, it seems like the mass shift is smaller the more matter the decay pions traverse. This means that the pions are loosing energy in the material due to ionisation so that the invariant mass of the pion-pion system becomes smaller. Then two errors, i.e the positive mass shift that was mentioned in section 6.2.1 and the energy loss in the target material, would cancel each other. However, to draw any conclusions from this, a rigorous study of Monte Carlo events is needed.

6.3.2 Armenteros plot

In Figure 29 the Armenteros plot for K_S^0 mesons decaying inside the target region is shown. The sample contains many $\gamma \to e^+e^-$ events at low values

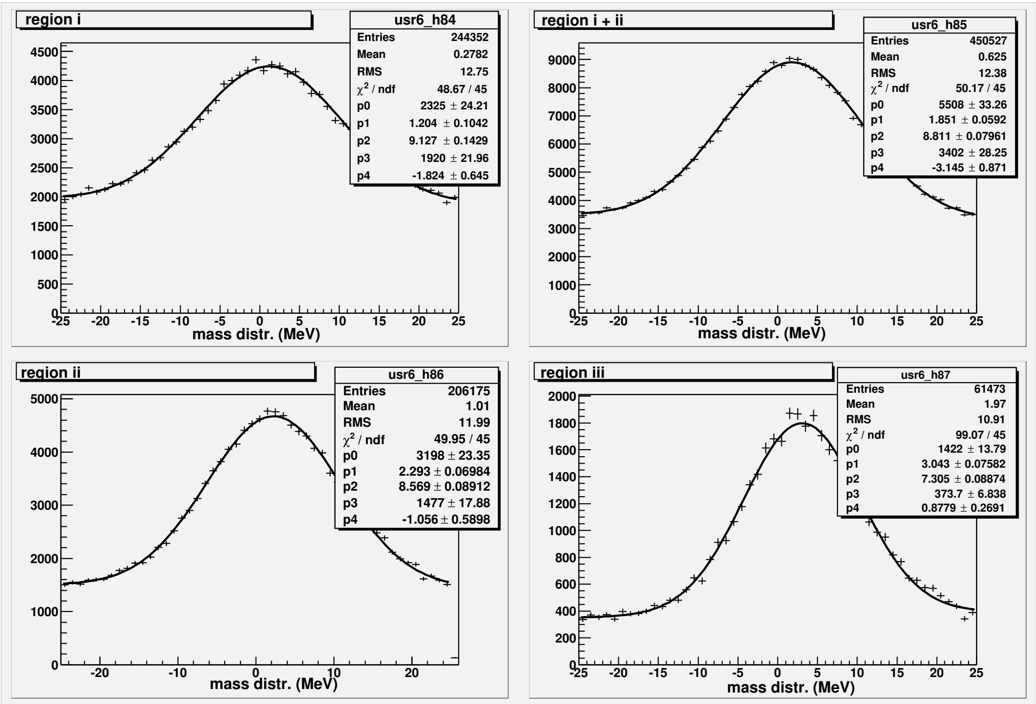

Figure 28: The mass distribution for K_S^0 mesons decaying in region i, i+ii, ii and iii, respectively. The regions are defined in the text, and the curves show the fitted fuctions, i.e. Gaussian curves folded with linear backgrounds.

Table 8: The signal to background ratio S/B, the mass resolution σ and the mass shift Δm for the radial regions defined in the text

Quantity	region i	region i + ii	region ii	region iii
S/B	0.55	0.71	0.92	1.40
σ (MeV)	9.13 ± 0.1	8.81 ± 0.08	8.57 ± 0.07	7.31 ± 0.09
Δm (MeV)	1.20 ± 0.1	1.85 ± 0.06	2.29 ± 0.07	3.09 ± 0.08

of p_t but is clean for higher values. This sample also contain some $\rho \to \pi^+\pi^-$ events, which can be seen from the vague half ellipse with a higher maximum value of p_t. For $\rho \to \pi^+\pi^-$ decays this value is 358 MeV [9].

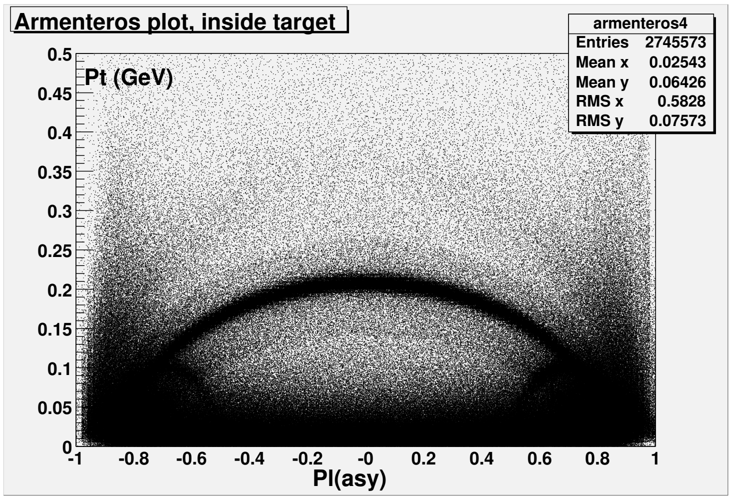

Figure 29: The Armenteros plot for K_S^0 mesons decaying inside the target. No mass cut is applied except for the one in the preselection, see section 5. The vague half-ellipse above the one corresponding to K_S^0 decays consists of $\rho^0 \rightarrow \pi^+\pi^-$ events.

Table 9: The mass error calculated from the track parameters, defined as the mean value of the dm distribution, together with the RMS of the dm distribution compared to the measured mass resolution σ. All these values are obtained for K_S^0 mesons decaying inside the target region.

dm mean (MeV)	dm RMS (MeV)	σ (MeV)
5.5	3.8	7.85 $\pm$ 0.04

6.3.3 K_S^0 mass resolution calculated from TrafDic errors

The error in the invariant mass is calculated in the same way as described in section 6.2.3. However, in this case the errors in the track parameters obtained from TrafDic also account for the fact that the pions undergo multiple Coulomb scattering in the material in the target, the target container and the target windows. From the distributions of the dmp, dmcos and dm, defined in section 6.2.3, it is clear than the mean values of dm and dmcos are indeed larger in this case compared to the case when the K_S^0 decay outside the target, as exspected, see Figure 30. The mass error inside the target is dominated by the multiple Coulomb scattering, that makes the error in the angle larger. However, the calculated errors are still smaller than the measured ones as can be seen in Table 9.

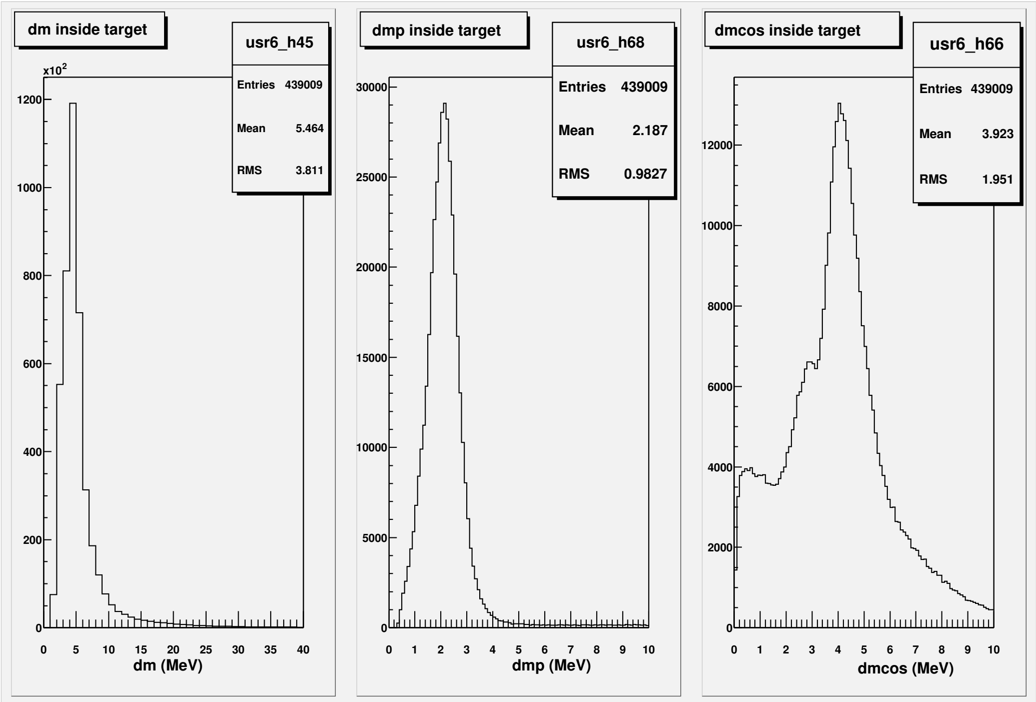

Figure 30: Left: The total mass error dm calculated from track parameters. Middle: dmp. Right: dmcos.

6.4 The K_S^0 run dependence

The COMPASS data are taken in runs of about 30 minutes. Conditions such as target solenoid current, beam intensity, target thickness and trigger might be different in different runs, which affects the results. When this analysis was performed, data from all runs in period P2D were not yet available.

6.4.1 The K_S^0 mass distribution run dependence

The shift in the K_S^0 mass and the mass resolution vary slightly depending on the run. The run dependence of these parameters are shown in Figure 31. Generally, the mass resolution tend to be worse and the mass shift larger for those runs where the solenoid current is negative, which means, for period P2D, that the upstrean target cell is positively polarised and the downstream negativley polarised with respect to the beam.

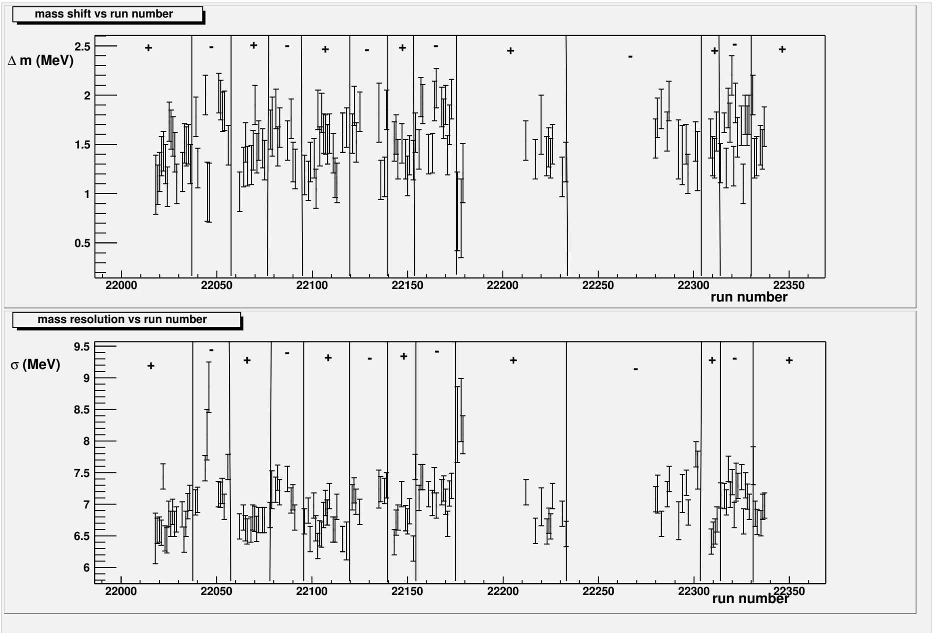

Figure 31: Top: The shift in the K_S^0 mass versus the run number in period P2D. Bottom: The mass resolution. The plus and minus signs indicate the sign of the target solenoid current and the vertical lines show when its direction is changed.

6.4.2 The K_S^0 yield run dependence

One way of studying the detector efficiency is to compare the amount of measured good K_S^0 events to the amount expected from Monte Carlo simulations. The number of measured good K_S^0 mesons is calculated for each run, normalised to the total number of events in each run and shown in Figure 32. The K_S^0 yield fluctuates around 0.46% except in runs 22176-22179 when the yield is lower. Monte Carlo data were not yet available when this study was done and therefore, no comparison has been made.

7 SUMMARY AND OUTLOOK

In this study, the spectrometer performance and the event reconstruction procedure were analysed using the sample of K_S^0 mesons produced in the 160 GeV polarised muon scattering off a polarised deuterium target in the COMPASS experiment at CERN. As a consequence, several problems in the hardware and software functioning were found. Some of them are solved, while a continuation of this analysis is suggested to solve others. A rigorous study of different cuts on the total sample has resulted in the following

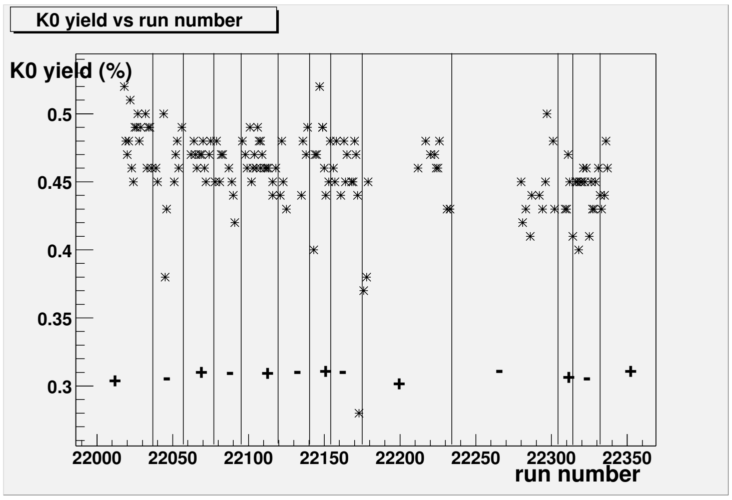

Figure 32: The K_S^0 yield versus the run number in period P2D. The plus and minus signs indicate the sign of the target solenoid current and the vertical lines show when its direction is changed.

definition of a good K_S^0 event:

- It contains a primary vertex.
- It contains a V^0 located at least 20 cm downstream the primary one.
- The invariant mass of the outgoing particles in the V^0 vertex, assumed to be pions, differs from the K_S^0 mass by at most 0.025 GeV.
- If $z(V^0) > 56$ cm, the angle $\Delta\theta$ between the momentum vector of the pion-pion system and the line connecting primary and V^0 vertex must be smaller than 0.04 radians.
- If $z(V^0) < 56$ cm, then $\Delta\theta$ must be smaller than 0.01 radians.

The sample is divided into two classes:

1. $z(V^0) > 56$ cm
2. $z(V^0) < 56$ cm

Of the total sample, 58 % of the events belong to class 1 and 42 % to class 2. From the 144 runs in the 2002 data taking period P2D and DST4 production included in the analysis, 492300 good K_S^0 events were found. Of those, 28 % are produced in the upstream target cell and 49 % in the downstream. The remaining ones are produced outside the target material, e.g. in the target gas mixing chamber, in the walls and windows of the target containers and in the detector planes. About 10 % of the measured K_S^0 mesons decay within the target cells, whereof 13 % decay in the upstream and 87 % in the downstream cell.

The reconstructed mass of the K_S^0 meson is shifted with respect to the PDG value. For class 1, the shift is (2.80 ± 0.03) MeV for tracks ending in the LAS, (-1.65 ± 0.03) MeV for tracks ending in the SAS and (1.26 ± 0.02) MeV for tracks ending anywhere in the spectrometer. For class 2, the mass shift is (2.01 ± 0.03) MeV for tracks ending anywhere in the spectrometer. The total mass shift varies depending on the run. Generally, the shift is larger for runs where the target solenoid current was negative.

The mass error calculated from track parameters is smaller than the measured mass resolution for both classes of K_S^0 events. For class 1, the calculated mass error is 3.7 MeV while the measured mass resolution is (6.02 ± 0.03) MeV. For class 2, it is 5.5 MeV compared to (7.85 ± 0.04) MeV. This means that the error of track parameters need a deeper investigation. The measured mass resolution is generally worse for runs where the solenoid current was negative.

The K_S^0 yield is fluctuating around 0.46 % of the total number of events depending on the run. No obvious dependence on the sign of the target solenoid current was found.

An error in the vertex reconstruction procedure was found. Hits from the beam muon were misinterpreted as hits from scattered muon for events where the primary interaction takes place within and downstream of the RICH1. This lead to a false estimation of the muon momentum and the primary vertex position. The error has now been corrected for.

Many important problems have been observed and solved 'online' during this analysis. The method of using K_S^0 events for studying the spectrometer performance and the data reconstruction is evidently very efficient. Therefore, a continuation of this study is needed for the future COMPASS data analysis.

8 ACKNOWLEDGEMENTS

First I would like to thank Barbara Badelek for her excellent supervision. Tack!

Many thanks also to Sergei Gerassimov, Yann Bedfer, Jean-Marc Le Goff and Alexandre Korzenev in the COMPASS collaboration for helpful advice during my work, and to Linus Andersson in the ISOLDE collaboration, my human LaTeX manual.

The TTA Technotransfer and the Wirsell Foundation, who provided me the financial means to stay and work at CERN, deserve my deepest thankful thoughts.

Last but not least, I want to thank Oscar Soederlund, my friends at CERN, in Sweden and elsewhere for support and advice in the world not connected to physics. May the force be with you!

References

[1] SLAC, M.J. Alguard *et al.*, Phys. Lett. 37 (1976) 1258; Phys. Rev. Lett. 37 (1976) 1261; Phys. Rev. Lett. 41 (1978) 70

[2] EMC, J. Ashman *et al.*, Phys. Lett. B206 (1988) 364; Nucl. Phys. B328 (1989) 1

[3] SMC, R. Windmolders, Nucl. Phys. Proc. Suppl. 79 (1999) 51

[4] COMPASS A Proposal for a COmmon Muon and Proton Apparatus for Structure and Spectroscopy, CERN/SPSLC 96-14 (1996)

[5] R. Windmolders, Proceedings of the workshop 'Spin in Physics', Villa Gualino, Turin, Italy, edited by M. Anselmino, F. Mila, J. Soffer, Frontier Group (2002) 93; also available as hep-ph/0211350

[6] COMPASS, J. Ball *et al.*, Nucl. Instr. and Meth. A 498 (2003) 101

[7] S. Dalla Torre, talk given at the workshop 'Future Physics at COMPASS', CERN (2002), 'http:/pccosrv1.cern.ch/compass/detector/rich/rich_locked/COMPASS_future/paper'

[8] B.R Martin and G. Shaw 'Particle Physics', John Wiley and Sons (1997)

[9] Particle Data Group, Phys. Rev. D50 (1994) 1201

[10] J. Podolanski, R. Armenteros, Philosophical Magazine 45 (1954) 13

[11] Y. Bedfer, 'http://y.home.cern.ch/y/ybedfer/www/RD2002'

[12] J-M Le Goff, COMPASS note 2000-13 (2002)